Geological concept revision during appraisal drilling: a replay of the McLeod VMS deposit, Matagami

Jef Caers

Stanford Mineral-X, Department of Earth and Planetary Sciences, Stanford University, Stanford, CA 94305, USA

Corresponding author: jcaers@stanford.edu

ORCID: https://orcid.org/[AUTHOR: ORCID iD]

This manuscript is a non-peer reviewed preprint submitted to EarthArXiv. It has been submitted for publication in *Ore Geology Reviews*. Subsequent versions of this manuscript may have different content. If accepted, the final version will be available via the DOI link on this page.

Geological concept revision during appraisal drilling: a replay of the McLeod VMS deposit, Matagami

Jef Caers

Stanford Mineral-X, Department of Earth and Planetary Sciences, Stanford University, Stanford, CA 94305, USA.
Corresponding author: Jef Caers, jcaers@stanford.edu

Abstract

Appraisal drilling is designed around a geological concept, yet discovery records show that such concepts are often partly wrong and revised late. We propose a procedure that updates the geological concept during drilling and quantifies the cost of delayed revision. The concept is written as a lattice of geological elements, each present or absent with a prior weight, so that revision becomes Bayesian inference over their combinations. A surprise score, the discrepancy between an observation and the prediction of the current model, locates where the data contradict the concept. The approach is tested by replay on the McLeod Zn–Cu volcanogenic massive sulfide (VMS) deposit, Matagami, Quebec. A reference model is built from the complete drilling record, and the deposit model of 2004 is rebuilt from the information available at that date. Three campaigns of similar cost drill the reference model from the 2004 state: the program drilled in 2005, a program planned on the five exclusive hypotheses of 2004 kept fixed, and a program planned on the lattice with sequential updating. Under the fixed hypotheses, drilling converged on the wrong hypothesis and ended at 0.9–1.0 Mt against a 3.0 Mt reference, with the value of delineation at 0–3 MCAD, close to walking away. The lattice ended at 2.5–3.4 Mt and valued delineation at 35–109 MCAD. The principal benefit of revision lies in a better quantification of economic potential and model uncertainty, more than in savings on drilling cost.

Keywords: concept revision; value-of-information; volcanogenic massive sulfide; Bayesian inference; replay; McLeod; Matagami

1. Introduction

Demand for copper, nickel and cobalt is projected to rise through 2040 in all three scenarios of the International Energy Agency (IEA, 2024), while the cost of each discovery has risen and the rate of discovery has fallen (Schodde, 2023). Mines that started production in 2020 to 2023 took almost 18 years from discovery (S&P Global Market Intelligence, 2024). This paper deals with the appraisal stage, between the discovery hole and the resource estimate that informs a development decision, where most of the drilling meters of a project are spent. A drill hole measures grade and thickness at one location; it also tests the geological concept the hole was planned on. The second is the subject of this paper.

Drill targeting is guided by a deposit-scale conceptual model: the geologist's hypothesis of the elements of the deposit, their spatial relations and the processes that produced them. An element is one component of that hypothesis, an ore lens on a marker horizon, a feeder root below it, a fault that displaces it. The mineral-systems approach formalizes the practice by resolving a deposit into source, pathway, trap and preservation and turning each into targeting criteria (McCuaig et al., 2010; Kreuzer et al., 2008). The deposit as drilled is the product of ore formation and of what followed it: deformation, intrusion, alteration and weathering overprint the primary expression, so that in a volcanogenic massive sulfide (VMS) district, the setting of this paper, a lens on a marker horizon may be folded, displaced by a fault, cut by sills and dikes and wrapped in a chlorite alteration halo.

At the outset of an appraisal the concept rests on a few drill holes, so it is usually wrong in part: elements the holes did not cross are omitted or assumed. The discovery record says revision is the usual outcome. At San Manuel the orebody was taken as complete for two decades until Lowell (1968) inferred its continuation across a fault and Kalamazoo was found; at Lalor a 2003 hole cut stringer sulfides four years before a hole under a second geophysical anomaly cut the first zinc lens (Newton and Vowles, 2017); at Olympic Dam the sediment-hosted model took eight to ten years to replace (Reynolds, 2000). To understand how successful revisions were made, we compiled about forty historical cases (Section 4).

A concept that is usually wrong in part needs a deposit model that contains uncertainty about the concept as well as about its parameters. Uncertainty in a deposit model is currently represented in two ways. Within one concept, geostatistical simulation draws many realizations of grade, thickness or geometry that honor the drilling, and their spread states the uncertainty of the parameters (Scheidt et al., 2018). Implicit structural modeling extends this to the geometry of horizons and faults, by perturbing the input data or by Bayesian inference on the parameters of a structural model (de la Varga and Wellmann, 2016; Wellmann and Caumon, 2018). Uncertainty about the concept itself is represented by a short list of alternative interpretations, each modeled separately and weighted by its fit to the data. Examples are the geological scenarios of petroleum reservoirs (Park et al., 2013) and the alternative conceptual models of hydrogeology, combined by Bayesian model averaging (Rojas et al., 2008; Refsgaard et al., 2012). Linde et al. (2015)

review how such prior geological knowledge enters inverse problems. In mineral exploration, prospectivity mapping weights evidence layers derived from a deposit model (Bonham-Carter, 1994).

Drill targeting and appraisal drilling are planned in three ways. The most common is expert judgment, guided by the deposit concept and by prospectivity maps (Hronsky and Groves, 2008). The second places drill holes where a geostatistical model is most uncertain, at the largest kriging or simulation variance of grade or of a mineralization boundary. The locations are found by heuristic optimization (Soltani-Mohammadi et al., 2021) or by Bayesian optimization (Jafrasteh and Suárez, 2021). The third values a drill hole by the decision it informs. Value-of-information analysis scores proposed drill data by the expected improvement in a development decision (Bratvold et al., 2009; Eidsvik et al., 2015). Applied to drilling, it values infill holes by their effect on the mine plan (Froyland et al., 2018) and exploration holes by their effect on the decision to mine or walk away (Eidsvik and Ellefmo, 2013). Sequential versions choose one hole at a time and update the model after each. They are posed as a partially observable Markov decision process (Mern and Caers, 2023) or through the sequential efficacy of information (Li et al., 2026). Most of these methods choose holes on one deposit model or on a fixed set of scenarios. Mern et al. (2024) plan under uncertainty about the model itself, and Wei et al. (2026) test whether drilling and geophysics falsify a geological hypothesis. A method in which drilling revises the concept element by element, with the cost of a fixed concept measured against a known outcome, is still missing.

This paper therefore addresses the following question: how should a geological concept be written so that drilling revises it, and what does keeping it fixed cost? The concept is written as a set of discrete elements, each present or absent, in a Bayesian deposit model that predicts every observation before it is made; the prediction is compared with the outcome, their discrepancy is the surprise (Bredehoeft, 2005; Box, 1980; Oreskes et al., 1994; Tarantola, 2006), and revision is inference on which elements the data support. The set of all combinations of the elements, each with a prior probability, is the lattice of concepts. The lattice revises within a fixed mineral system; a change of system, a post-ore overprint or a re-timing of structures is outside its scope. The lattice itself is not a new statistical idea. Each element is an indicator with a prior probability of inclusion, and the posterior over all possible combinations is a Bayesian variable selection, the spike-and-slab prior of Mitchell and Beauchamp (1988) and George and McCulloch (1993). A model whose number of components is inferred is trans-dimensional, the space the reversible-jump samplers of geophysical inversion sample (Malinverno, 2002; Sambridge et al., 2006; Bodin and Sambridge, 2009). The new step is to translate these ideas to mineral exploration and appraisal and to place them in a decision framework on a real case. The end goal is a decision: how to spend exploration dollars and whether to proceed or walk away.

The method is tested by replay (Section 3). The case is McLeod, a zinc-copper VMS deposit of the Matagami district, Quebec: a copper occurrence from 1960, a 14 m intercept in 2004, a discovery hole in 2007 and a mine with Bracemac from 2013 (Carr and Roy, 2011). The replay starts at the end of 2004 and covers the season in which the real concept changed.

The paper makes three contributions. It reviews about forty documented concept revisions and their lags (Section 4). It writes the concept as a lattice of elements, in which revision is inference and a surprise score from the model's own predictions marks where the concept is contradicted (Section 5). It measures by replay on McLeod what a fixed concept costs against a revisable one (Sections 3 and 6).

2. The McLeod deposit

The Matagami district lies in the Abitibi greenstone belt of Quebec, a bimodal Archean volcanic pile: the Watson Lake Group rhyolite and dacite at the base, the Key Tuffite, and the Wabassee Group andesite and basalt above (MacGeehan, 1978; Clark, 1983; Figure 1a). The Key Tuffite is a laminated chert-tuff marker, a tuff with an exhalative component, 0.1 to 10 m thick at Bracemac-McLeod (Liaghat and MacLean, 1992; Genna et al., 2014). It is traced throughout the south flank with 1 to 2% Zn near the deposits; it records a hiatus in volcanism and the deposits sit at or near it (Adair, 2009; Ross et al., 2014). The deposits are tabular or mound-shaped lenses of pyrite, sphalerite and chalcopyrite at or just below the Key Tuffite, formed on and below the sea floor over roots in chlorite-talc pipes (Adair, 2009; Genna et al., 2014; Pierre et al., 2016). Many deposits have both parts. Eleven were found from 1957 by electromagnetics; ten had been mined by 2004, 44.3 Mt at 8.8% Zn and 0.87% Cu (GM 61688). Bell Allard, found in 1992 (Adam et al., 1997), was mined at 950 to 1,025 m and showed that ore continues along the horizon far below the historic holes. Synvolcanic gabbro sills and dikes inflate the pile and cut the sulfides (Sharpe, 1968; Adair, 2009; Pierre et al., 2016). Till covers the district; on the south flank the horizon strikes northwest and dips 45° as a district average and 60 to 68° at McLeod.

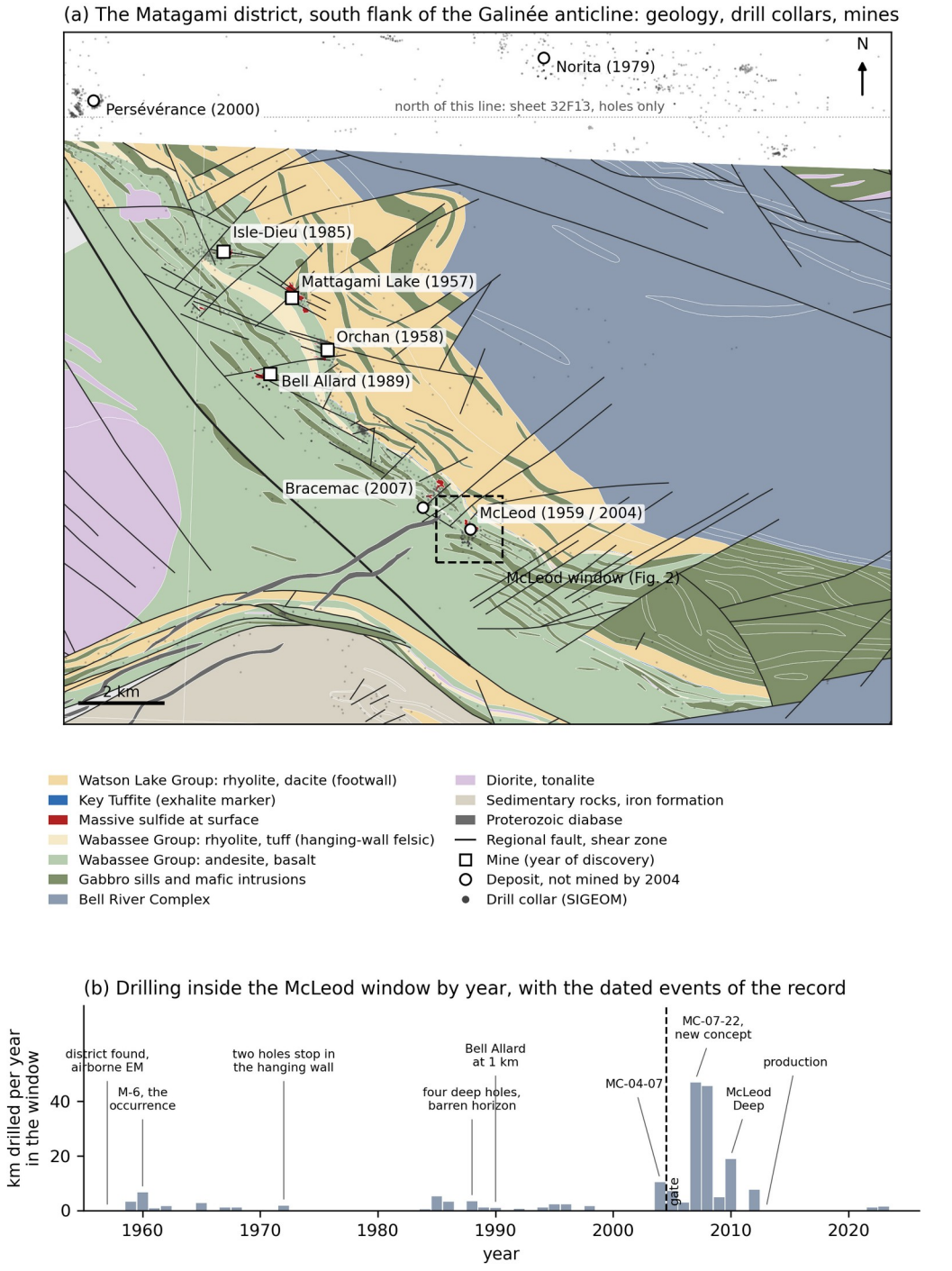


Figure 1. The Matagami district and the McLeod record. (a) Geology of the south flank of the Galinée anticline (SIGEOM 1:50,000, sheet 32F12): footwall rhyolite and dacite, the Key Tuffite, hanging-wall basalt and andesite, the Bell River Complex, the gabbro sills and the regional faults, with the drill collars, the mines, the two deposits of the Bracemac-McLeod property with their year of discovery, and the 1.6 km McLeod window of Figure 2. (b) Meters drilled per year inside the window, with the dated events of the record and the gate at the end of 2004.

McLeod was a copper occurrence for forty-four years (Figure 1b; Table 1). In 1960 hole M-6, on a magnetic structure, cut 6.95 m at 4.21% Cu and 1.17% Zn at about 220 m, stringers with small massive sections in chlorite-talc alteration (GM 09221). Twenty-nine holes around it to 1968 did not outline a zone, and the

option lapsed (GM 13311; GM 20511; GM 22303). In 1972 two of three Asarco holes to the horizon at depth stopped in the Bracemac rhyolite, a hanging-wall unit taken for the footwall (GM 28608). In 1988 Cominco drilled four vertical holes, 3,678 m, to the horizon at 700 to 900 m between McLeod and Bracemac; three cut barren Key Tuffite and one 22 cm of magnetite (GM 47941; GM 49061), and the claims lapsed in 1999. Two errors of this period matter to the analysis: a hanging-wall unit was misassigned, and the horizon was assumed continuous and barren between four deep crossings. Each program tested one concept and stopped when it came up empty.

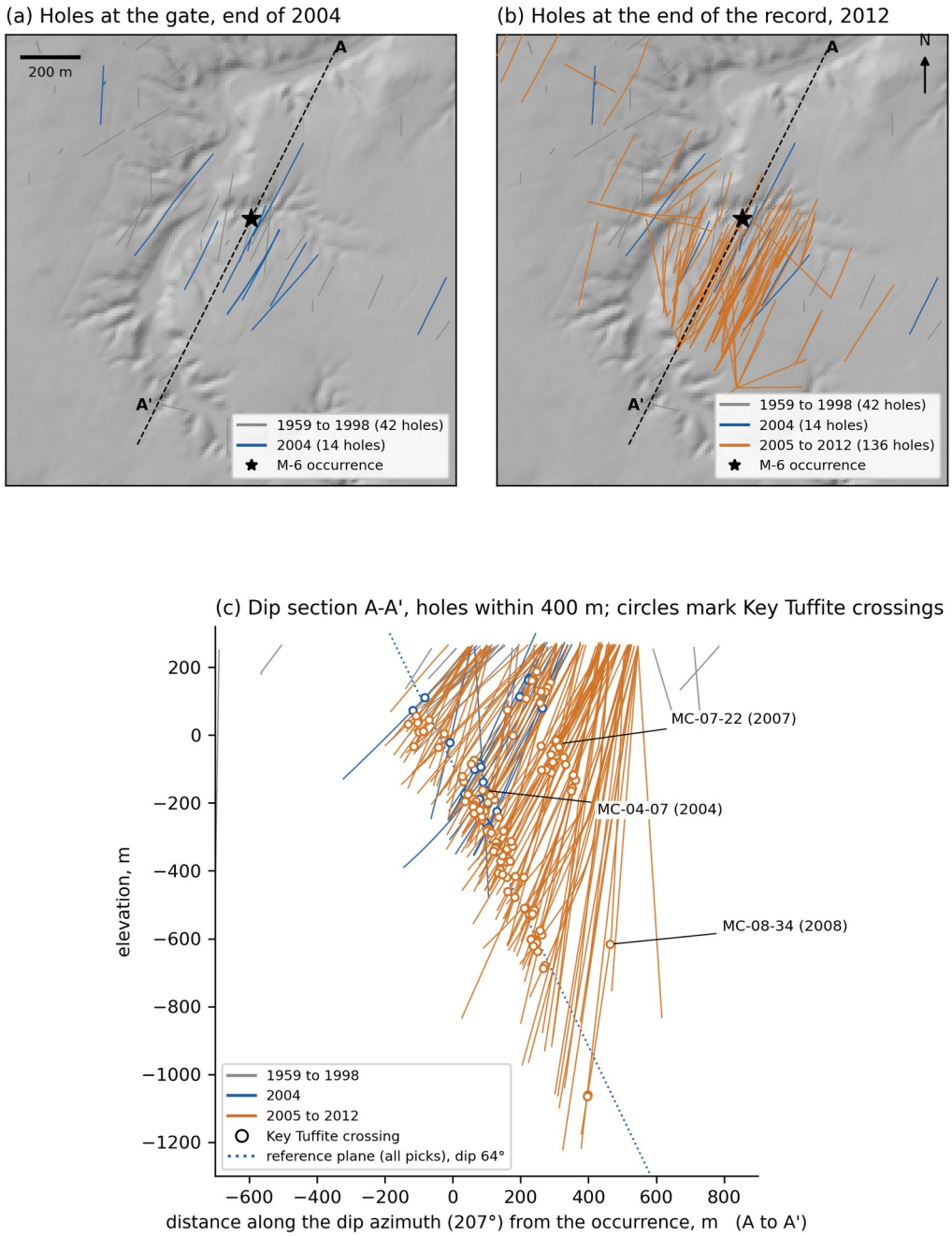


Figure 2. The drilling of the McLeod window. (a) Collars at the gate, end of 2004: the 42 holes of 1959 to 1998 and the 14 of 2004, on the LiDAR hillshade; 37 of the 42 and all 14 of 2004 fall in the model window of Appendix F. (b) The window at the end of the record in 2012, with the 136 holes of 2005 to 2012. (c) Dip section A-A' through the M-6 occurrence along azimuth 207°, with the holes within 400 m of the section and the Key Tuffite crossings as circles; MC-04-07, MC-07-22 and MC-08-34 are named. The dotted line is the plane fitted to all crossings, dip 64°.

Three conditions shaped exploration at McLeod. The orebody is concealed under cover, so concepts were tested by drilling almost alone. Borehole electromagnetics detected 20 to 30% of the sulfides later intersected, even in its three-component form of 2006 to 2008, because the sulfides conduct poorly (Adair,

2009). Target selection followed the concept in force: magnetic structures in 1960, the projected horizon at depth in 1988, the occurrence and then a geophysical anomaly in 2004. The drilling is public, in the assessment and technical reports. A deposit model can therefore be rebuilt for any year and checked against what was drilled afterwards. Section 3 builds the replay on this record.

Table 1. The exploration phases at McLeod, from the assessment reports and the 2009 technical report.

Phase	Years	What was known	Stated aim	How it ended
Detection	1959 to 1960	District deposits found by EM; two magnetic structures on the property	Test the structures for sulfides	M-6: 6.95 m at 4.21% Cu, the occurrence
Outline	1960 to 1968	One intersection on the horizon	Delimit the zone; test the horizon east and west	Twenty-nine drill holes; the option lapsed
Horizon at depth	1972; 1988	The horizon continues down dip; deep ore elsewhere in the district	Test the Key Tuffite at 700 to 900 m	Two drill holes short of the horizon (1972); three barren crossings (1988); claims lapsed 1999
Re-test	2004 to 2005	The occurrence, its stratigraphy, pulse EM in the hole	Confirm, step out along the horizon, follow the geophysics	MC-04-07: 14.05 m at 11.15% Zn; follow-up did not find the footprint of a 5 Mt body (GM 64243); metal prices depressed (Adair, 2009)
New concept	2006 to 2007	Three stated fundamentals; three-component borehole EM	Find developable ore beyond Perseverance	Bracemac (January 2007); MC-07-22 at McLeod
Delineation	2007 to 2008	Two zones on the horizon; stacked sulfides; a stringer zone	Delineate at 50 m spacing	3.62 Mt indicated (February 2009); the fault, the window, the sills recognized
Definition and depth	2009 to 2012	An indicated resource	Measured category; roots; depth	McLeod Deep (2010); production 2013

3. The replay

3.1 The concept of replay

The purpose of replay is to be able to evaluate new decision-making processes and the use of new technology on well-documented historical cases. Replay rebuilds, from the records of the time, the deposit model available at a chosen date, with its uncertainty. The framework comprises three components: (i) a reference “as-found” deposit model (Section 3.3; Appendix F) that can be virtually drilled and logged at arbitrary locations and orientations; (ii) a time-stamped evidentiary ledger (Appendix A) listing all information that a site geologist could have accessed by the replay date, including the source document for each item; and (iii) an information-control gate that exposes only the ledger entries and drill data available up to the specified date and withholds everything later. The gate keeps what an analyst knows in 2026 from the geologist of 2004.

The replay starts in the winter of 2004 to 2005, after drilling of MC-04-13 and before MC-05-14. The program the operator drilled that winter is nine drill holes, seven collars and two wedges, 6.6 km of core, 0.83 MCAD at the 2004 rate. Every campaign of Section 6 starts from this date and from the same deposit model.

3.2 Conceptual geological uncertainty in 2004

Pre-2004 syntheses describe a VMS deposit with a few recurrent elements (Franklin et al., 1981; Lydon, 1984, 1988; Large, 1992; Franklin, 1996; Gibson et al., 1999; Galley, 2003). The orebody is a stratiform lens of massive sulfide on a marker horizon that persists beyond the deposit, as a mound over a focused vent or as a thin extensive sheet where brines ponded, the Besshi type as the sheet end member (Slack, 1993). Below the lens a discordant altered footwall pipe, chlorite-cored and cut by stringer feeders, is a common component of the system (Franklin et al., 1981; Lydon, 1984). Where sulfides are abundant its stringer zone is denser than the host rock (Salisbury et al., 2000); ore concentrated in the pipe is a copper-rich root. Persistent systems stack lenses at more than one level; sills thicken the pile, dikes cut it, and the horizon may be folded and faulted after burial.

Between 1968 and 2000 the district's stratigraphy, alteration pipes, sills, stacked lenses and deep ore were documented. Noranda, the operator, had mined the district since 1963. The ledger of the gate (Table A.1) lists what a geologist of 2004 could know at McLeod, item by item with its source. Its key entries are the property dip of 60 to 68°, the barren crossings of 1988 at 700 to 900 m, and the 13 holes of 2004, among them MC-04-07 (14.05 m at 11.15% Zn) and the stringer conduit in MC-04-08 (GM 61688).

The dataset comprises 132 drill holes completed in the McLeod window by the end of 2004, including 19 holes drilled with a Key Tuffite pick. A barren hole constrains the lens along its trace. The drilling reports state the exploration target of each hole drilled in 2004 and 2005. Combined with the district geological model and the exploration history of the property, these targets define the five hypotheses of the operator (Figure 3). The hypotheses and their evidence come from the record. Their weights are our interpretation of the 2004 program.

H1, mound model (prior probability = 0.40): a mound or sheet of massive sulfide on the horizon at the occurrence, of unknown extent. It is the district's reference genetic model (Sharpe, 1968; Roberts, 1975) and was the main target of the 2004 drilling.

H2, feeder-root model (prior probability = 0.20): the occurrence is a small discordant root in an alteration pipe, with the related mound elsewhere on the horizon, as at Mattagami Lake (Roberts and Reardon, 1978; MacGeehan, 1978), Isle-Dieu (Lavallière et al., 1994) and Perseverance.

H3, cut horizon (0.20): faults or mafic dikes offset or truncate the horizon near the occurrence, which would explain missing or displaced crossings. District faults were mapped (Sharpe, 1968; Beaudry and Gaucher, 1986). The first fault on the property was recognized in 2008.

H4, stacked lenses (0.10): lenses at a higher tuffite level in the Wabassee Group, as mapped in the district (Sharpe, 1968), drilled at Orchan (Clark, 1983) and typical of the class (Gibson and Watkinson, 1990). The 2004 logs describe stringers and chloritized rhyolite above the horizon.

H5, system at depth (0.10): ore continues down dip below the historic holes, as at Bell Allard (about 1 km; 1992) and Norita East (600 to 900 m; 1985), where seismic traced the Key Tuffite to 1,440 m (Adair, 2009;

Adam et al., 1997, 2003). The four barren crossings of 1988 at 700 to 900 m lowered its weight from 0.25 to 0.10.

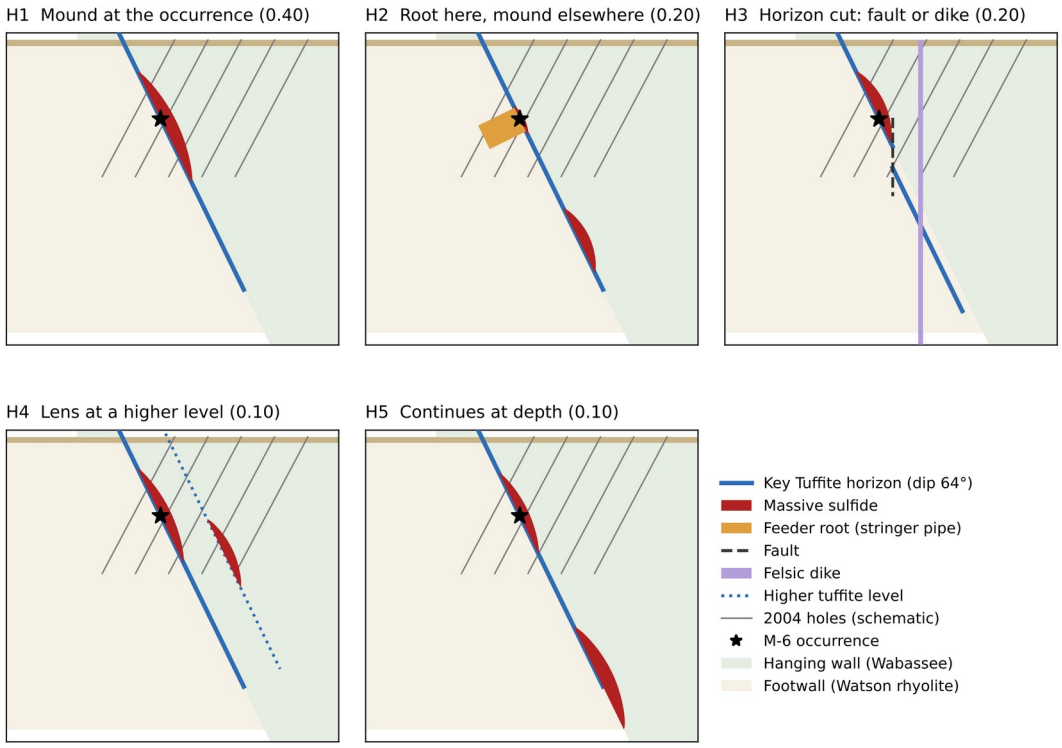


Figure 3. The five hypotheses of the winter of 2004 to 2005, as dip-section sketches with the weights of the ledger: H1 a mound on the horizon at the occurrence; H2 the occurrence as a small feeder root with the mound elsewhere along the horizon; H3 the horizon displaced or cut by a fault or a dike; H4 lenses at a higher tuffite level in the hanging wall; H5 the system continuing at depth below the historic drill holes. H1 keeps the lens at the occurrence; H2 to H4 add their element to the horizon and leave the lenses to the district's rate; H5 places its lens down dip. The gray lines stand for the 2004 drill holes, schematic.

The VMS literature and the 2004 record name three further elements that a geologist writing the McLeod concept could have listed and the 2004 targets did not: the sheet, the flexure and the halo (Figure 4). The sheet is a thin stratiform body extending along the horizon, the tabular end member of the class (Lydon, 1984; Large, 1992), documented at Rosebery (Large, 1992) and in Besshi-type districts (Slack, 1993). The 1960 drill holes cut thin zinc intervals near the horizon beside the copper stringers of M-6. A Noranda geologist of 2004 would have ranked a thin sheet below a mound, since the district's thickest ore sits at its largest tonnages, so the element takes the weight of the operator's least-preferred hypotheses, 0.10.

The flexure is a bend of the horizon along dip within the drilled window. The horizon is the limb of a plunging anticline with local dip variation (Beaudry and Gaucher, 1986; Piché et al., 1993), steep to vertical at Norita on the north flank. On the property the depth of the horizon is known at two levels, 200 to 600 m from the 1960s and 2004 holes and 700 to 900 m from the 1988 holes, so the dip between the levels can be compared with the dip within each. The pre-2004 reports do not document a bend at McLeod; the element takes 0.10.

The halo is the altered footwall under the occurrence: the alteration pipe common to the class, with a chlorite core enriched in iron and magnesium. On the property it was logged twice before the gate, in M-6 in 1960 and in the conduit of MC-04-08; its density was first measured in 2007, so the 2004 model takes handbook values (Telford et al., 1990). The element takes 0.10. Gabbro sills have stronger pre-2004 support than any of the three (Sharpe, 1968; Adam et al., 1997, 2003) and were logged in 2004; they are placed in every world of the deposit model and are not a switch. Table 2 summarizes the 2004 record on the district's lenses and the Key Tuffite surface. Table 3 lists the seven elements, the prior probability that each is present and the ranges of their parameters. Section 5.3 turns these into the prior of the deposit model.

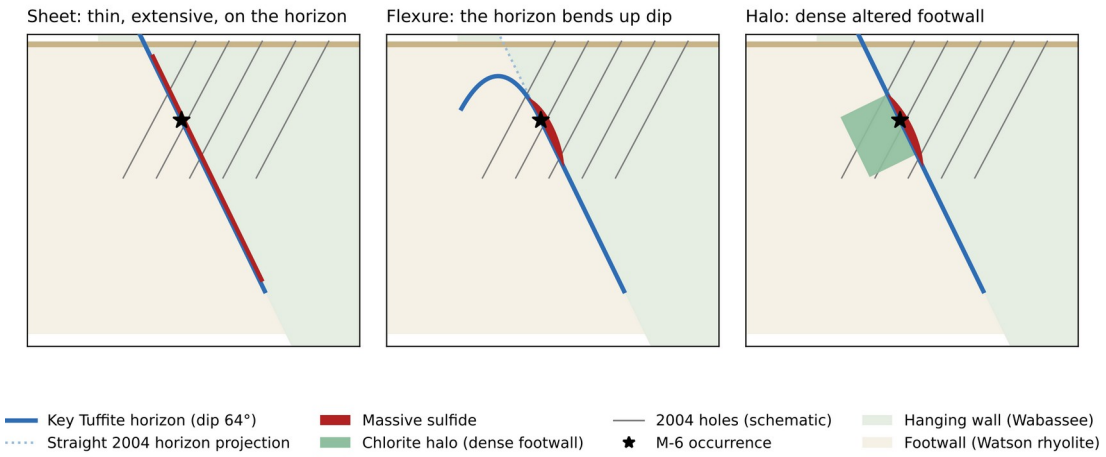


Figure 4. The three further elements of the 2004 record, as dip-section sketches in the idiom of Figure 3: the sheet, a thin extensive body of massive sulfide on the horizon in place of a mound; the flexure, the horizon bending up dip below its straight projection (dotted); the halo, a zone of dense altered footwall under the occurrence.

Table 2. The 2004 prior: the base lens and the Key Tuffite surface.

Quantity	Prior or value
Base lens tonnage	lognormal, median 1.8 Mt (fitted to the 11 deposits known by 2004)
Base lens length-to-thickness	10 to 60
Base lens Zn grade	near 9.5%
Base lens Cu grade	near 0.9%
Key Tuffite strike	117 plus or minus 15 degrees
Key Tuffite dip	60 to 68 degrees
Surface undulation, vertical spread	5 to 25 m
Surface undulation, lateral range	200 to 800 m
Elements added beyond the era concept	any number of the seven; the mound stays in every world

Table 3. The seven elements of the 2004 concept, their prior probability of being present and their parameter ranges.

Element	Prior w	What it adds	Parameters and ranges
Fault	0.20	Offsets the surface down dip	Position down dip; throw 0 to 100 m
Feeder root	0.20	Extends the lens into a pipe below the horizon	Position; depth; radius
Second level	0.10	A lens at a higher tuffite level	Level above the horizon; size
Deep lens	0.10	A lens down dip beyond the historic drill holes	Position down dip; size
Sheet	0.10	A thin extensive body on the horizon, free of the	Length; width; thickness (meters)

Element	Prior w	What it adds	Parameters and ranges
		size rule	
Flexure	0.10	Bends the surface at two hinges on the dip line	Two hinge positions; slope up to 19 degrees
Halo	0.10	Raises the footwall density under the occurrence	Excess 0.02 to 0.15 t/m3; footprint; thickness 20 to 150 m

3.3 Geological concept today

The deposit geometry and continuity, as defined by drilling between 2006 and 2012, are summarized in Figure 5; the corresponding reference model constructed on 20 m cells is provided in Appendix F. Mineralization comprises a laterally extensive, thin sheet of massive sulfide situated on the Key Tuffite, with an estimated resource of 3.01 Mt grading 12.3% Zn. The sheet persists down-dip from the 2004 zone, extending through the Lower zone intersected in drillhole MC-07-22 (2007) to McLeod Deep, 1,085 to 1,385 m below surface (Carr and Roy, 2011). A sub-vertical fault at the base of the 2004 zone, about 600 m below surface, drops the Lower zone about 50 m and separates it from the Upper zone (GM 64243; Adair, 2009). A laterally continuous copper stringer zone, surrounded by a chlorite alteration halo, underlies the massive sulfide horizon and is interpreted to be continuous with the 1960 occurrence and the 2004 feeder/conduit system. Stratigraphically, the mineralized horizon exhibits an up-dip flexure proximal to the occurrence, occurring below the linear projection of the 2004 horizon.

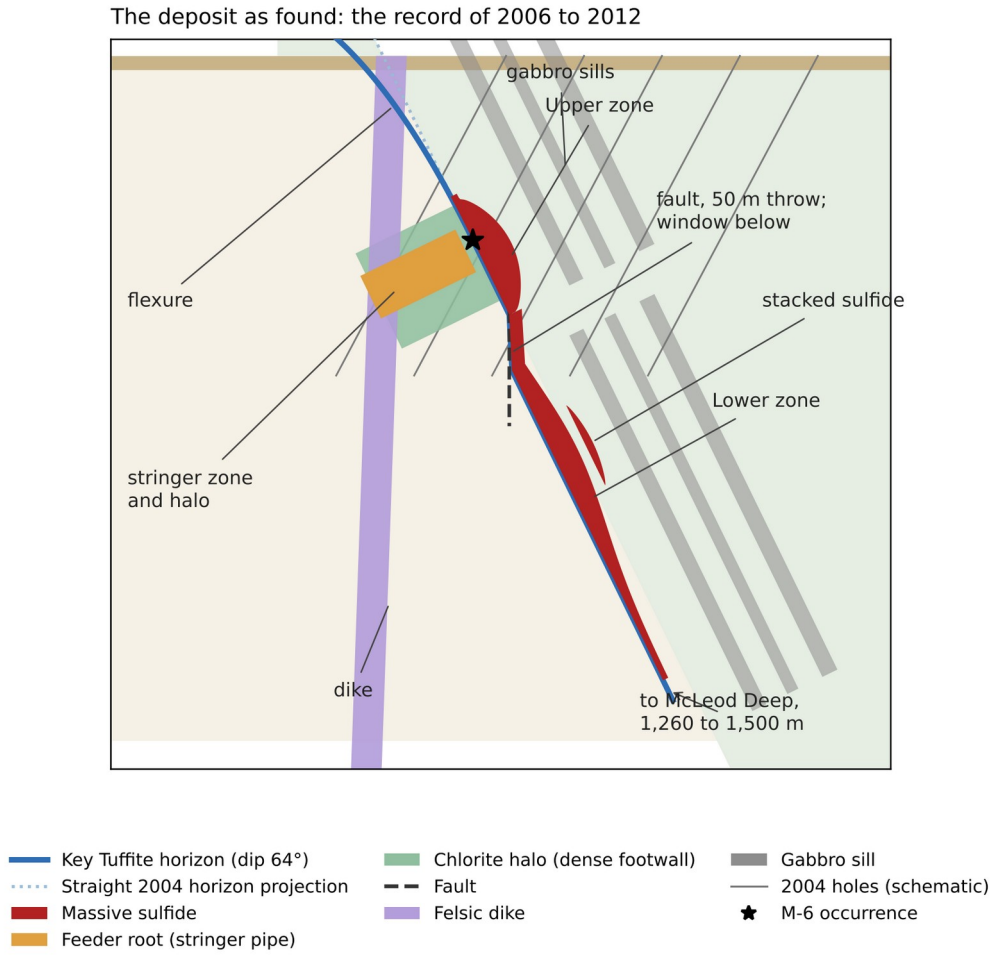


Figure 5. The deposit as the record of 2006 to 2012 describes it, in the idiom of Figure 3 (the full 3D reference model is built in Appendix F): the massive-sulfide sheet with the Upper and Lower zones; the fault with its 50 m throw and the window below it; the stringer zone and chlorite halo under the occurrence; stacked sulfide above the horizon; the gabbro sills and the felsic dike in the hanging wall; the horizon bending up dip below the straight 2004 projection; the continuation toward McLeod Deep.

Each hypothesis proposed in 2004 identified only one of these elements. The deposit has all of them. The sheet, the halo, the flexure and the sills were absent from every hypothesis of 2004. The exploration concept that led to its discovery, articulated by Donner and Xstrata in 2006, rested on three premises: (i) sulfide can occur at levels above the main horizon where alteration is present above it; (ii) roots in pipe facies have small footprints; and (iii) weak electromagnetic anomalies can mark ore, because sulfides in the district are poor conductors (Adair, 2009).

4. What the exploration record shows about concept revision

McLeod is one instance of a general pattern: the concept of 2004 changed only in 2006, with a new team. To see how often concepts are revised, and how, we compiled about forty documented discoveries and re-discoveries, porphyry, VMS, orogenic gold, iron oxide copper-gold and unconformity uranium, from the discovery case histories of the Society of Economic Geologists, SMEDG, AusIMM and Exploration 97 and 17, from technical reports and from the deposit monographs. A case entered when its authors state the

concept before and after and describe the revision; for each we recorded the prior concept, what prompted the revision, its type, the lag from the contrary evidence to the revised concept, and the outcome. The catalog is conditioned on success, since programs that kept a wrong concept and failed leave few histories. A full account of the sources is provided in supplementary information.

We found from this literature that revision is one of thirteen types, eleven recurring, defined in Table 4 with an example each. Seven keep the mineral system and change one element or structure: RE-PARAM changes the geometry, depth or size of elements present (Bell Allard; Adam et al., 1997); ADD-ELEMENT adds a root, a stringer zone, a stacked or deeper lens; CONNECT joins two known bodies (McLeod; Carr and Roy, 2011); ADD-STRUCT adds a fault, thrust, fold or tilt (Carlin; Roberts, 1960); RESTORE inverts a structure to predict the missing part (San Manuel; Lowell, 1968); CORRELATE-ACROSS matches a marker across a structure (West Wits; Krahmann, 1936); RE-TIME changes the age of a structure relative to the ore. Four change the system or the explanation of its data: ADD-OVERPRINT, a post-ore process (Olympic Dam; Ehrig et al., 2021); RE-ATTRIBUTE, a geophysical response assigned to a different body with the ore unchanged; SWAP-SYSTEM; and COMBINE, as at Far Southeast-Lepanto (Hedenquist et al., 1998). SPLIT (Fosterville; Voisey et al., 2020) and RE-WEIGHT, the re-scoring of archived data (Disini et al., 1998), occur once each.

Table 4. The eleven recurring types of concept revision found in the record, with one documented example each.

Type of revision	What changes in the concept	Example	Source
RE-PARAM	Geometry, depth, plunge or size of the same elements	Bell Allard: the Key Tuffite targeted at 1 km	Adam et al., 1997
ADD-ELEMENT	A new component of the same system: root, stringer zone, stacked or deep lens	Lalor: stringer, then zinc lenses, then gold and Cu-Au zones	Newton and Vowles, 2017
CONNECT	Two known bodies joined into one system	McLeod: the 2004 and 2007 zones joined in 2008	Carr and Roy, 2011
ADD-STRUCT	A fault, thrust, fold set or tilt added	Carlin: ore in windows beneath the Roberts Mountains thrust	Roberts, 1960
RESTORE	A structure inverted to predict the missing part	Kalamazoo: the missing half of San Manuel projected across a fault	Lowell, 1968
CORRELATE-ACROSS	A marker matched across a structure to fix the offset	West Wits: magnetic shales traced under the dolomite cover	Krahmann, 1936
RE-TIME	The age of a structure relative to the ore changed	Mount Isa: copper ore placed before the Paroo Fault sealed and folded	Long, 2010
ADD-OVERPRINT	A post-ore process added	Olympic Dam: uranium added at 0.7 to 0.5 Ga	Ehrig et al., 2021
RE-ATTRIBUTE	A sensor response assigned to a different body	Ernest Henry: the TEM conductor was the supergene layer	Webb and Rowston, 1995
SWAP-SYSTEM	The mineral system replaced	Olympic Dam: sediment-hosted Cu replaced by a hematite breccia complex	Reynolds, 2000
COMBINE	Elements of two deposit models joined in one system	Far Southeast–Lepanto: porphyry Cu-Au and the overlying high-sulfidation enargite ore shown to be one evolving system	Hedenquist et al., 1998

The record shows three patterns. First, most revisions are incremental and draw on a small set of known elements. In the VMS examples, revisions changed depth, lateral offset, plunge or connectivity.

Substitutions of the mineral system came mostly by analogy to other districts (e.g., Cadia; Holliday et al., 1999; Century; Rebek, 2007).

Second, revision comes long after the first surprising drilling. Several cases take decades: 20 years at Kalamazoo, 45 years at McLeod, 50 at Buchans (Thurlow, 1981), and 95 years at Broken Hill (Marjoribanks et al., 1980). After the revision, discovery took little drilling: the third hole at Carlin, a single re-entered hole at West Wits.

Third, surprising observations were often absorbed into the prevailing hypothesis by small ad hoc changes. For example, the Olympic Dam group kept a modified sediment-hosted model after the first breccia intersections (Roberts and Hudson, 1983); at Fosterville, a deep gold intercept judged immaterial was not followed up for five years (Phillips, 2022); and Hunt (2002) presents the Lihir experience as a warning about the inertia of successful models. Interpretation experiments suggest the mechanism: interpreters draw on a small set of concepts and anchor on their first hypothesis (Bond et al., 2007, 2012; Alcalde et al., 2017, 2019).

The record is therefore evidence of how revisions should be made, and that they can be done in a much shorter time period. First, revision should start with a set of geological elements that could have been proposed at that time and these elements are then added sequentially (i.e., one addition per revision step). Second, each revision type is treated as an independent modification supported by revision-specific evidence: for example, ADD-STRUCT is evaluated using a depth residual, whereas ADD-ELEMENT is evaluated using a stringer intercept. Third, a revised concept must be geologically plausible as well as fit the data. Interpreters of seismic sections who checked that their structure could be restored and could have formed in sequence were about three times more likely to be correct (Bond et al., 2012).

5. Method

The method follows the requirements of Section 4. Its elements come from what a geologist of 2004 could list (Sections 5.1 and 5.2). Its prior keeps every revised concept within ranges a geologist of 2004 would accept (Section 5.3). Each element is revised by the drilling evidence it predicts, with every hole scored again (Section 5.4). Section 5.5 chooses the holes.

5.1 Geological model conceptualization

At McLeod the massive sulfide lies on, or just above, the Key Tuffite. Every intercept that constrains the ore comes from a hole that crosses this marker. The deposit model is therefore built outward from the horizon. A “world” is one internally consistent realization of the deposit that a geologist of 2004 could have drawn: the Key Tuffite surface, the massive-sulfide bodies on it and the elements of the concept. The deposit model is an ensemble of 2,000 worlds. Its model uncertainty is the spread among them.

Each world has its own frame (Figure 6), the complete model details and values extracted from the ledger as well as their sources are listed in Appendix A & B. The stratigraphic anchor horizon corresponds to the Key

Tuffite intersected in borehole M-6. A plane passes through the anchor with the strike σ and the dip δ of the world, drawn about the ledger's 117° and 64°. A position on the horizon is given by two coordinates on that plane, u along strike and v down dip. A height is the distance w perpendicular to the plane. The horizon departs from the plane by the sum of four terms,

$$H(u,v) = w_0 + Z(u,v) + F(v) + \tau\, n_z 1\left[v > v_c\right], \tag{1}$$

The offset w_0 places the horizon above or below the logged position of the occurrence, within the error of that pick. The undulation Z is a smooth random surface that represents the local dip variations of the marker. It has a lateral range l, the distance over which two points of the surface stay correlated, and a vertical spread σ_Z. It is zero at the occurrence. The flexure F is zero unless the flexure is switched on. It bends the horizon at two hinges on the dip line, v_1 and v_2, with one slope up dip of the first hinge and another down dip of the second. The last term is the fault, also zero unless it is switched on. Down dip of the line $v = v_c$ the fault displaces the horizon by a vertical throw τ. The factor n_z, the vertical component of the normal to the plane, converts the throw into a displacement perpendicular to the plane.

Massive sulfide mineralization is represented on this surface as a set of discrete bodies. Each body is parameterized as a half-ellipsoid positioned on the horizon, defined by a centroid, two semi-axes, an orientation, a maximum thickness, an estimated tonnage, and individual zinc and copper grades (Figure 6a). In all realizations, a mound lens is emplaced within 300 m of the occurrence (H1 in Figure 3). Additional lenses are introduced along strike at a rate consistent with the district discovery rate.

Subsequent components of the conceptual model are superimposed on this base configuration. The "root" component introduces additional sulfide mineralization in the footwall directly beneath the occurrence. The second level adds a lens at a tuffite stratigraphic level above the horizon; the "deep lens" introduces a body down-dip of the historic drill holes; and the "sheet" component adds a thin, horizon-parallel body extending along strike

At each intersection between the drill trajectory and a geological horizon, the model yields two predicted quantities: (i) the position of the intersection expressed as depth along the drill hole, and (ii) the expected logged sulfide interval length at that location. The latter is the true thickness divided by the cosine of the angle between the hole and the normal to the horizon. The information contributed by a drill hole is quantified by comparing these model-based predictions with the observed drill log (Section 5.4; Appendix C.1).

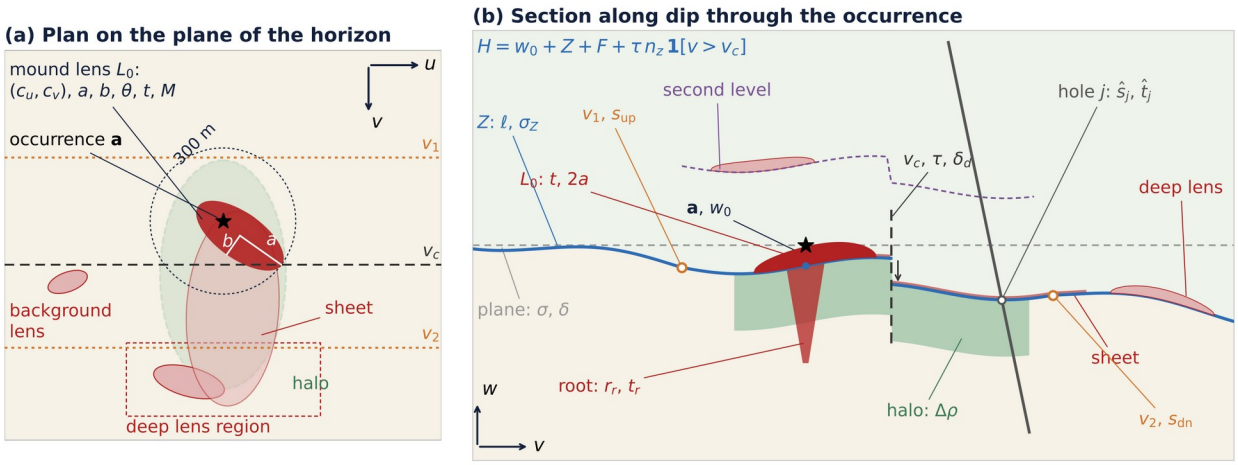


Figure 6. A world of the deposit model, built from the Key Tuffite surface. Schematic, with positions and sizes inside the prior ranges of Table 3 and Table B.1. (a) The plane of the horizon seen from above, u along strike and v down dip from the occurrence a (star). L_0 is the mound lens with center (c_u, c_v), semi-axes a and b, orientation θ, maximum thickness t and tonnage M; its center lies within the dotted 300 m circle. A background lens, the sheet, the region of the deep lens and the footprint of the halo are shown with the lines of the fault (v_c) and of the hinges of the flexure (v_1, v_2). (b) A section along the dip line through the occurrence, drawn in the frame of the plane with heights w exaggerated 1.7 times. The dashed gray line is the plane with strike σ and dip δ. The blue line is the horizon H of equation (1): the offset w_0 at the occurrence, the undulation Z with range l and spread σ_Z, the hinges v_1 and v_2 with slopes s_{up} and s_{dn}, and the fault at v_c with throw τ and dike width δ_d. On the horizon lie the lens, the sheet and the deep lens. Below it lies the root, with radius r_r and thickness t_r, and the halo with its density excess $\Delta\rho$. Above it lies the second level (dashed purple). A drill hole j crosses the horizon at the open circle, where the world predicts the crossing depth $\hat{s}_j$ and the apparent sulfide length $\hat{t}_j$.

5.2 The lattice: a revisable geological modeling concept

In our approach, a concept may be modified via two principal mechanisms: (i) reweighting the hypotheses already embedded within it, and (ii) expansion, whereby an additional hypothesis is introduced. The latter corresponds to the stage in Box's iterative cycle that follows an anomalous observation and is termed "model expansion" by Gelman and Shalizi (2013).

To let the concept gain or lose elements, we define a lattice of binary "switches" (Figure 7). Each of the seven elements listed in Table 3 is associated with a binary switch s_k, which takes the value 1 when the element is present and 0 when it is absent. A concept is thus represented by the 7-dimensional binary vector s comprising these switches. The resulting lattice contains $2^7 = 128$ distinct concepts. The concept in which all switches are off corresponds to the base case (H1), i.e., the mound at the occurrence. The 2004 hypotheses correspond to base concepts with exactly one switch activated: H3 includes the fault, H2 includes the root, H4 includes the second level, and H5 includes the deep lens. The other concepts, absent from the 2004 targets, combine these elements or add the sheet, the flexure or the halo.

The lattice differs from a list of 128 hypotheses in three ways. The geologist states seven weights, one per element, and the probability of each of the 128 concepts follows from them. A fault has the same throw and position in every concept that includes it. Evidence on the fault therefore applies to all of them. Concepts that differ by one element are neighbors. An update adds or removes one element and keeps the rest of the concept. Figure 8 draws two example routes as dip-section sketches, the route to the reference concept and a route the 2004 feeder-root interpretation could have taken.

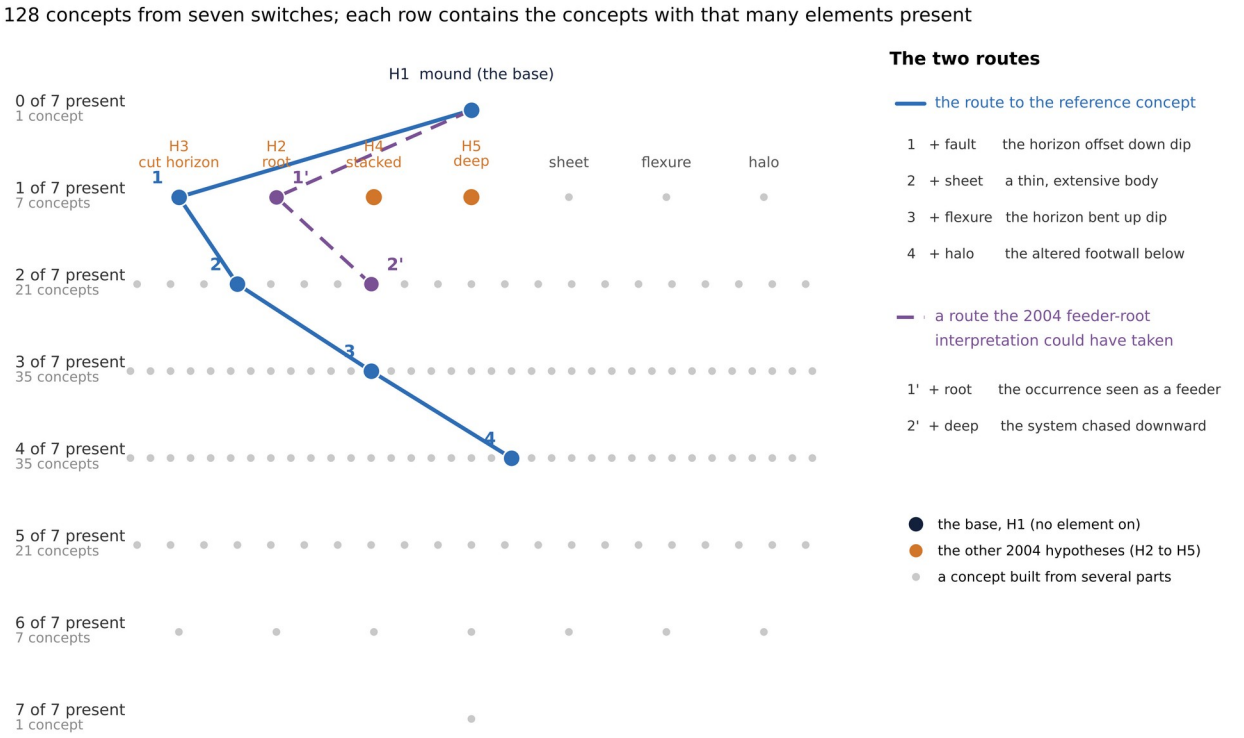


Figure 7. The lattice of concepts: 128 concepts from seven switches, in rows by the number of elements present. The base is H1 of Figure 3; the single-element concepts of the fault, root, second level and deep lens add to that base what H3, H2, H4 and H5 name, with the mound kept; the sheet, flexure and halo are the further elements of Section 3.2. Blue, steps 1 to 4: the route from the base to the reference concept. Purple dashed, 1′ and 2′: a route the 2004 feeder-root interpretation could have taken.

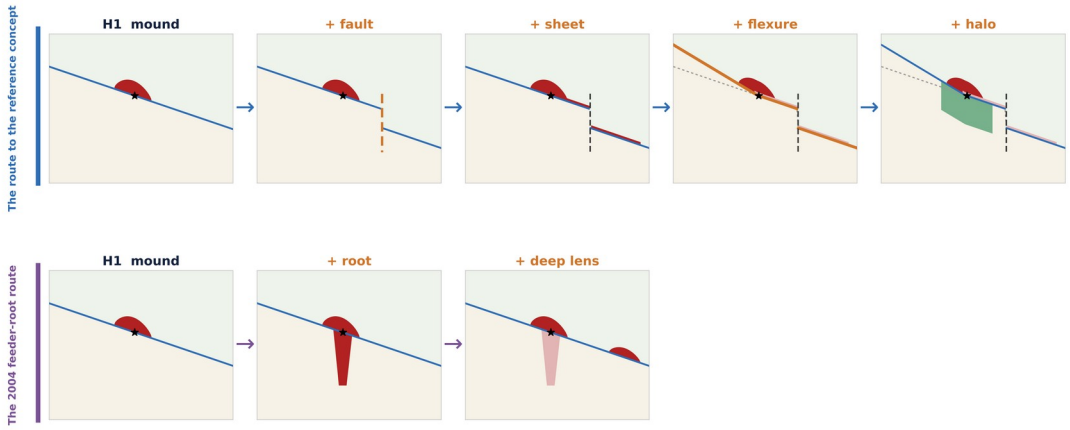


Figure 8. Two routes through the lattice of Figure 7 as dip-section sketches, each panel adding one element. Top, the base to the reference concept: the mound, then the fault, the sheet, the flexure and the halo. Bottom, the feeder-root route: the mound, a root beneath the occurrence, a deep lens down dip. Red massive sulfide; green the chlorite halo; dashed the fault; dotted the straight 2004 projection of the horizon; orange the element switched on at that step.

5.3 The prior distribution of model parameters

Bayesian inference requires a prior: the probability a geologist of 2004 gives each concept and each parameter before new drilling. The prior for this case has three parts, each taken from the record of 2004 (consult Appendix B for full details, we cover the essential only here). The base world follows Table 2: the attitude of the Key Tuffite, the smoothness of its undulation, and the size, shape and grades of the district's lenses fitted to the eleven deposits known by 2004. The switches follow the weights of the elements,

$$p(s) = \prod_{k=1}^{K} w_k^{s_k} \left(1 - w_k\right)^{1 - s_k}, \tag{2}$$

with $K = 7$ and w_k the era's weight on element k: 0.20 for the fault and the root, the weights the ledger gives hypotheses H3 and H2, and 0.10 each for the second level, the deep lens, the sheet, the flexure and the halo. Equation (2) treats the weights as independent probabilities of inclusion. The base concept receives 0.38 and the fault alone 0.09. About a third of the prior mass lies on concepts outside the operator's five. The fixed-concept campaign uses the operator's mutually exclusive weights of Figure 3. To prevent overfitting, this prior favors simpler models over more complex ones: a concept with few elements has a higher prior probability than one with many.

The third component concerns the parameterization of each model element, with values sampled from ranges that would have been defensible to a geologist in 2004. These ranges are summarized in Table 3, and the complete prior specifications are provided in Table B.1.

5.4 Updating the lattice and the worlds with each hole

Borehole data inform both the drilled intervals (direct data) as well as the geological concepts (indirect data). For example, consider a borehole intersecting the Key Tuffite at a depth 60 m below that predicted by the 2004 model. It constrains the depth and attitude of the horizon and tests the concept. The update therefore revises two things at once: (i) which elements are present and (ii) the values of their parameters.

The update acts on the ensemble of worlds of Section 5.1. The probability that element k is present is the share of worlds with its switch on. Given the data D it follows from Bayes' rule,

$$p(s_k=1 \vee D)=\frac{w_k\, p(D \vee s_k=1)}{w_k\, p(D \vee s_k=1)+(1-w_k)\, p(D \vee s_k=0)}, \tag{3}$$

where $p(D \mid s_k=1)$ is the probability of the data averaged over all worlds with the element present, their other switches and all parameters included, and $p(D \mid s_k=0)$ is the same average over the worlds without it. The ratio of the two averages is the Bayes factor of the element. An element becomes more probable present than absent when its Bayes factor exceeds $(1-w_k)/w_k$. For example, a Bayes factor of 4 (for the fault) indicates that the observed logs are four times more probable under the model that includes the fault than under the model without it.

Figure 9 illustrates the steps of a single update of the ensemble. The upper panel depicts the sequence of a single action cycle, whereas the lower panel traces six of the 2,000 realizations ("worlds") through the same cycle. Prior to drilling the borehole, each realization generates predictions of the intersection location between the borehole trajectory and the Key Tuffite, as well as the expected sulfide logging interval at that stratigraphic unit. The probability of an observation y under a world m is the likelihood $p(y \mid m)$. Averaged over the worlds given the data so far, the likelihood gives the predictive distribution of the log,

$$p(y \vee D)=\int p(y \vee m)\, p(m \vee D)\, dm. \tag{4}$$

where $p(m \mid D)$, the posterior, is the probability of world m given the data D. Appendix C.1 presents the details of the likelihood model.

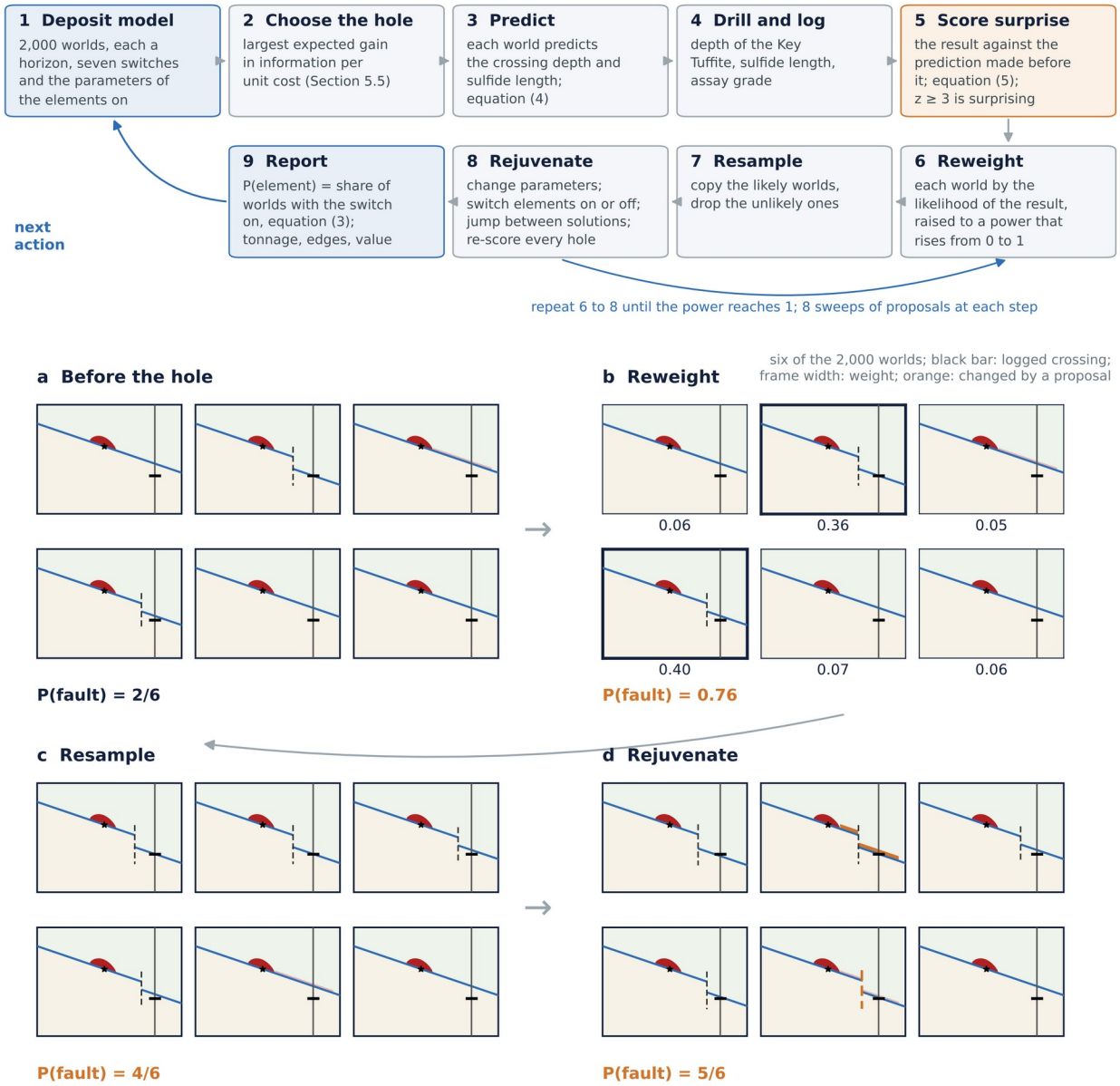


Figure 9. The update of the deposit model after each action. Top: the loop of one action, in which steps 6 to 8 repeat as the power of the likelihood rises from 0 to 1. Bottom: six of the 2,000 worlds through one update, schematic: (a) before the hole, (b) after reweighting, (c) after resampling, (d) after rejuvenation. A hole (gray line) logs the Key Tuffite below its straight projection (black bar). Reweighting raises the weight of the worlds whose fault drops the horizon to that depth (frame width; weights under the panels). Resampling copies them. Rejuvenation changes their parameters and switches elements, here a sheet in one world and a fault in another (orange). The share of worlds with a fault, the probability of equation (3), rises from 2/6 to 5/6.

New data is first evaluated against the model's prior predictive distribution before any parameter or weight updates are performed. An observation assigned low probability under the ensemble's predictive distribution is treated as anomalous or unexpected. In the context of an exploration program, its primary function is to provide an early warning that the underlying conceptual model likely requires revision. Let $S(y)$ be the log predictive density of an observation y under (4). Simulating N outcomes y_1 to y_N from (4) gives the mean $\acute{S}$ and the standard deviation sd_S of S. The surprise of the observation actually made,

y_{obs}, is the z-score

$$z = \frac{S(y_{obs}) - \acute{S}}{sd_S}, \qquad (5)$$

The score is the number of standard deviations by which an observation is less probable than a typical outcome under the model in force. It is computed on the distribution predicted before the observation (the prior predictive). Under a correctly specified model the score has mean 0 and unit variance. The check therefore looks at the upper tail.

The log then enters the ensemble in three steps (Figure 9, steps 6 to 8; Appendix C). Reweighting multiplies the weight of each world by the likelihood of the log under that world. Worlds that predicted the log well gain weight. The likelihood enters in increments, so the weight stays spread over at least half of the worlds. Resampling copies each world in proportion to its weight. Worlds the hole contradicts disappear. Worlds it supports multiply. Without a further step the ensemble would shrink to a few distinct worlds and claim a confidence the data do not support. Rejuvenation therefore changes the copies by small proposed changes of four kinds: a parameter update changes the value of an element; a switch update turns an element on or off, a step to a neighboring concept on the lattice; a birth–death update adds or removes a background lens; a mixture update jumps between solutions that small changes cannot connect. Each proposal is accepted or rejected by the Metropolis–Hastings rule (Appendix C.5), which scores the proposed world by its prior and by its fit to all the drilling so far. An element or a lens enters only when its gain in fit outweighs its prior charge (Section 5.3). A world the data cannot yet exclude keeps its chance of being retained. The three steps repeat until the likelihood enters at full power.

5.5 Choosing where to drill

Our drill planner combines revision on the lattice with a reward for information to choose where to drill next. The value of an action is the expected improvement in the decision it informs, minus the cost of data collection, the value of information (Eidsvik et al., 2015). The decision at the end of the campaign is whether to delineate, to drill the lens at 50 m spacing to a resource or walk away. The value of delineating under a deposit model is the net value of the lens the model expects, at the metal prices and costs of 2004, minus the delineation program priced on the footprint the model expects, the 50 m grid over the expected extent plus the step-outs that find each edge (Appendix D). Let $V(D)$ be the value of the best terminal decision under the deposit model after data D: the larger of the value of delineating and zero. For an action a with cost c(a), the expected value of the information it brings is

$$EVI(a) = E_y\left[V(D \cup \{y\})\right] - V(D) - c(a). \qquad (6)$$

where the expectation is over the outcomes y of the action under the predictive distribution (4). The EVI values the terminal decision under the current deposit model; the reward that chooses the next action is stated next.

The planner drills one hole at a time, by the largest expected reward per unit cost, updates the model, and chooses again, with a one-step lookahead and without optimizing over the sequence of later actions. The term open-loop follows Mern and Caers (2023) and Caers et al. (2026). The reward of the campaigns of Section 6 is the expected reduction in the entropy of the deposit model over the ten quantities the operator reports, per unit cost; it is defined in Appendix D beside the expected value of information of equation (6), which chooses the same hole at most steps. The campaign stops after sixteen actions.

The planner chooses from a fixed menu of 35 targets on the 2004 plane of the Key Tuffite: seven along strike from −600 to +600 m and five down dip of the occurrence from 50 to 850 m, at the 200 m spacing of the 2005 program. Every hole is drilled at azimuth 030 and dip −65° and continues 150 m beyond its target. A hole costs C$125 per meter.

6. Results

6.1 How the results are evaluated

We compare three campaigns run from the deposit model of the end of 2004 (Table 5): the program the operator drilled in 2005; drilling planned on the five hypotheses of 2004 kept fixed; and drilling planned on the lattice.

Planning estimates the tonnage and the other quantities that enter the VOI. The VOI is therefore itself an estimate. A different seed of the random numbers can give a different result. To measure this sensitivity, each planner is run with three seeds. The program as drilled in 2005 is fixed and does not need a seed.

Table 5. The three campaigns. The five-concept model keeps the era's exclusive weights; the lattice has all seven switches.

Campaign	Deposit model	Data planned	Planner	Seeds
1. The program as drilled	five concepts; lattice	the nine drill holes of 2005 (seven collars and two wedges) in order	the operator's	1
2. Fixed concepts	five concepts, kept fixed	drilling	open-loop	3
3. Lattice, drilling	lattice, revisable	drilling	open-loop	3
control	lattice	drilling	open-loop	2

Each campaign is scored on the reference model with three groups of measures.

The first group measures what each campaign concludes about the deposit. *Size* is the expected tonnage of the terminal deposit model, the mean over its 2,000 worlds. *P size* is the share of the worlds whose tonnage falls in the class of the reference deposit, 2 to 5 Mt. A mean can approach the reference by averaging worlds that are all wrong. *P size* therefore tests whether the model puts its weight on deposits like the real one.

The second group measures the timing of revision, a key point we made based on historical cases. The surprise score of Section 5.4 is recorded after each hole. The first action with a score of 3 or more dates the first contradiction between the concept and the data. For the lattice, the first action at which the probability

of an element exceeds 0.5 and stays above it dates the revision itself. The terminal probability, equation (3), states where the concept ended.

The third group measures what that conclusion costs. *Spent* is the drilling cost at 2004 rates. The *value believed* is the net value of the lens the terminal model expects, minus the delineation program priced on the footprint the model expects. The terminal decision follows from it: delineate when the value is positive, walk away otherwise. The *value realized* scores that decision on the reference deposit. Values are given at the prices of 2004 and at the mean prices of 2013 to 2022, the years the mine produced, net of the delineation program and the spend.

6.2 Results

The results answer three questions: how close each campaign comes to the deposit, how early it revises its concept, and what the difference costs.

Does each campaign end with the right size of deposit, with its uncertainty placed on the right answer? The campaigns differ most on this question. The fixed hypotheses end at 0.9 to 1.0 Mt against the reference of 3.0 Mt, with 0.11 to 0.12 of their worlds in the reference class of 2 to 5 Mt (Table 6; Figure 10b). The lattice ends at 2.5 to 3.4 Mt, with 0.27 to 0.35 of its worlds in that class. The fixed model therefore converges with confidence on a deposit a third the size of the real one. The lattice comes within a sixth of the reference and puts nearly three times as much weight on the right size class. Scored on the lattice, the program as drilled ends at 2.0 Mt, with 0.12 of its worlds in the reference class.

The cause of the difference is the exclusivity of the five hypotheses. The holes below the occurrence cross the Key Tuffite deeper than the 2004 plane predicts. These depth residuals favor H3, the cut horizon. H3 passes 0.9 in every seed by 0.8 MCAD and ends at 0.99 to 1.00 (Figure 11a). H3 is right that the horizon is cut. As an exclusive hypothesis it also states that the ore at the occurrence comes only from the district’s background rate of lenses. Under H3 the barren crossings near drill hole MC-04-07 remove the lens from 35 to 43% of the worlds. The remaining worlds place a lens of about 1 Mt up dip or along strike. The depth residuals do not inform the ore. Exclusivity couples the two claims, so the evidence for the cut is counted as evidence against the ore.

The lattice keeps the two claims apart. The mound lens at the occurrence is part of every world. The fault is a switch added to it. The same residuals raise the probability of the fault above 0.5 within two holes in every seed. The lens stays where the 2004 assays put it.

Drilling resolves the tonnage better than the elements behind it. The fault ends at 0.07, 0.77 and 0.36 in the three seeds (Figure 11b). The two holes on the row 250 m below the occurrence cross the horizon at depths that a faulted plane and an undulating surface fit equally well at 200 m spacing. The 2005 program crossed the horizon on both sides of the fault in the same sections and resolved it. The sheet falls from its prior of 0.10 to 0.01 to 0.02. The reference deposit is a sheet, so the lattice reaches the right tonnage with the wrong

geometry: a larger mound lens whose grade is fixed by the assays. The root stays near zero from the start, rejected by the assays of 2004: 1.2% Zn at the occurrence against 11.4% in MC-04-07.

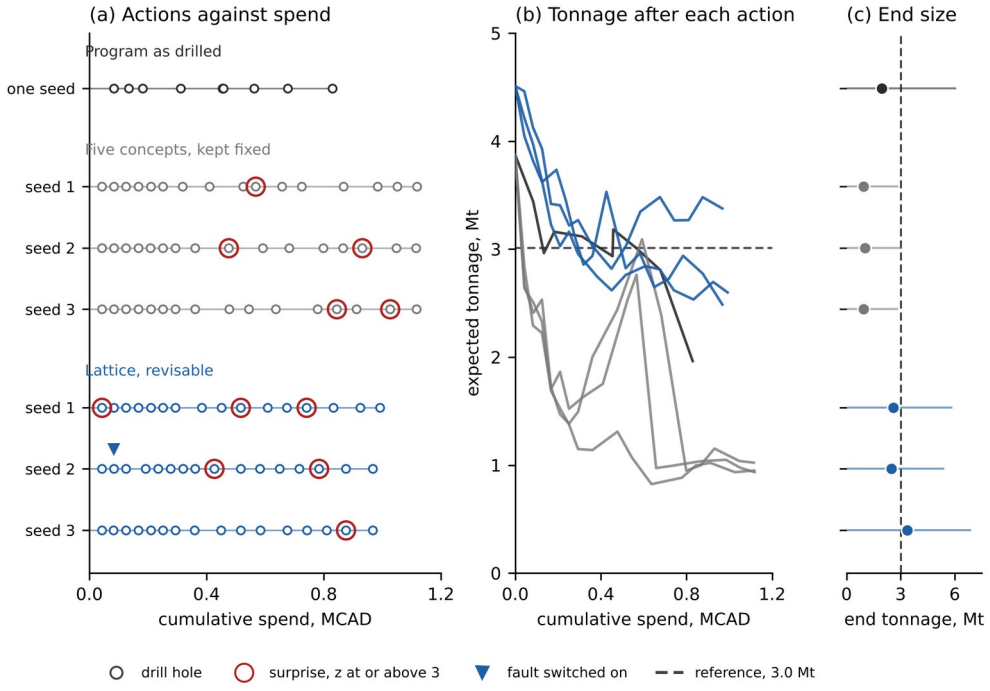


Figure 10. The three campaigns: (a) actions against cumulative spend in MCAD, one row per seed, drill holes as open circles, surprises (z at or above 3) ringed, the action at which the fault switched on and stayed on as a triangle; (b) the expected tonnage after each action against the reference 3.0 Mt (dashed); (c) the tonnage at the end with its standard deviation.

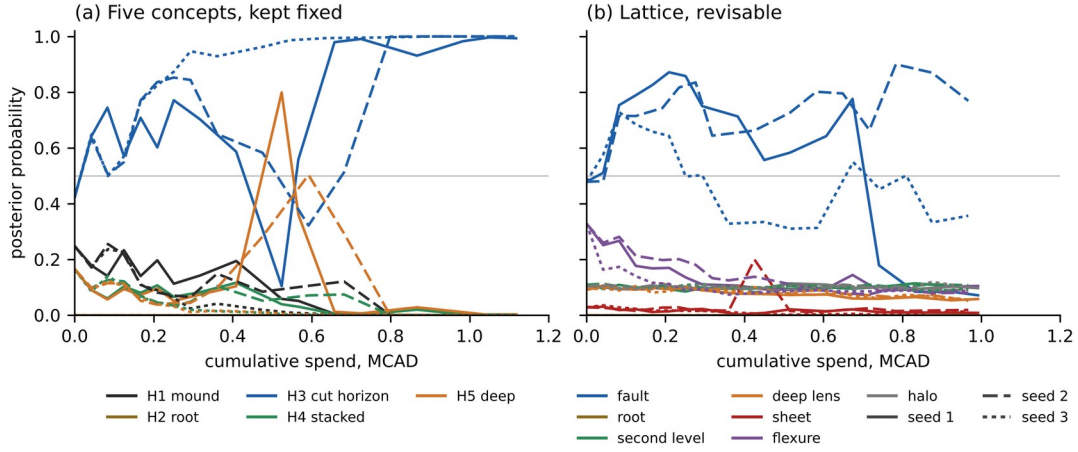


Figure 11. How the concept changed, three seeds each (solid, dashed, dotted). (a) The five fixed hypotheses: the posterior weight of each after each action; H3 reaches 0.99 in every seed by 0.8 MCAD. (b) The lattice: the posterior probability of each element; the fault passes 0.5 within two holes in every seed and ends at 0.07, 0.77 and 0.36. The root stays at zero and the sheet falls to 0.01 to 0.02. The flexure and the halo stay near their prior of 0.10.

How early was the concept revised? In the lattice-based campaign, the conceptual model was updated within two drill holes for each seed: the posterior probability of a model fault exceeded 0.5 by the second decision point (Figure 10a, triangles). The fixed-hypothesis campaigns met their first contradictory observations at decision points 9, 10, and 13, after spending 0.48 to 0.84 MCAD. Section 4 quantified the lag between discordant evidence and model updating in units of years; the replay analysis expresses the same lag in units of drill holes. On the lattice the lag was two drill holes. Under the fixed hypotheses the concept was not revised during the campaign.

Under the fixed hypotheses, the surprise score signals that the concept is misspecified. The earliest surprise events were detected at depths of approximately 250 m and 650 m below the occurrence. H3 reached a posterior probability of 0.99 because the five hypotheses did not include the pattern the observations imply: a fault beside a lens at the occurrence.

On the lattice, revision does not wait for a surprise. The first surprises came at actions 1, 9 and 15. For two seeds the fault switched on before any surprise. The surprise score then has a second role. It marks the contradictions that the lattice cannot absorb, and such a contradiction shows that the list of elements itself must be revised.

What does each campaign cost? The campaigns spent nearly the same: 0.83 MCAD for the program as drilled, 0.97 to 0.99 MCAD for the lattice and 1.11 to 1.12 MCAD for the fixed hypotheses (Table 6). Every campaign ends up with a terminal decision to further delineate the orebody. On the reference deposit every decision realizes 133 to 140 MCAD at 2004 prices and 635 to 641 MCAD at the prices of 2013 to 2022. The realized values differ mainly through the delineation program, priced on each model’s footprint: 22 to 25 MCAD for the planned campaigns and 31 MCAD for the program as drilled.

Hence, the difference lies in the model uncertainty behind the decision, not the cost of drilling. The fixed hypotheses value delineation at −0.4 to 3.1 MCAD net of their spend, at the edge of break-even: their 0.9 to 1.0 Mt sits just above the break-even tonnage of 0.81 Mt at 2004 prices. A small fall in the price of zinc or a small rise in cost turns their decision into walking away from a deposit that realizes 137 to 139 MCAD at the same prices. The lattice values the same decision at 35 to 109 MCAD. Its decision keeps a wide margin above break-even.

Table 6. The three campaigns on the reference model (3.0 Mt at 12.3% Zn). Spent in MCAD at 2004 rates; drilling in km of core; size the expected tonnage of the terminal model and P size the share of its worlds in the reference class, 2 to 5 Mt; value believed at 2004 prices and value realized on the reference model at 2004 prices (Zn 1.36 and Cu 3.73 CAD/kg; the reference deposit 163 MCAD) and at the mean prices of 2013 to 2022 (Zn 3.19 and Cu 8.45 CAD/kg; 665 MCAD), all net of the delineation program and the spend. Break-even at the reference grades: 0.81 Mt at 2004 prices, 0.25 Mt at those of 2013 to 2022. Ranges span the seeds.

Campaign	Seeds	Spent	Drilling km	Size Mt	P size	Value believed	Realized, 2004 prices	Realized, 2013 to 2022 prices	Decision
1. Program as drilled	1	0.83	6.6	2.0	0.12	39	133	635	delineate
2. Fixed concepts, drilling	3	1.11 to 1.12	8.9	0.9 to 1.0	0.11 to 0.12	-0.4 to 3.1	137 to 139	639 to 641	delineate
3. Lattice, drilling	3	0.97 to 0.99	7.7 to 7.9	2.5 to 3.4	0.27 to 0.35	35 to 109	138 to 140	640 to 641	delineate

The history of McLeod shows that this risk was real. The operator's follow-up of 2005 did not find the footprint of a 5 Mt body. Metal prices were depressed in 2005. The program stopped (Table 1; Adair, 2009). The concept changed only when the people changed. The joint venture of Donner Metals with Falconbridge, later Xstrata, reassessed the district in 2006 and stated the three premises of Section 3.3. Drilling under the new concept led to the Bracemac discovery in January 2007 and the McLeod lens in drill hole MC-07-22. The mine produced from 2013. The revision of 2006 required a new team and a new interpretation of the record.

7. Conclusion

This paper proposes replay as a retrospective test of new methods and technologies in mineral exploration (Section 3). Because the outcome of the deposit is known, a method can be scored after each action and at its terminal decision and compared with the geologists of the time on the same data. This evaluation is inherently constrained by the historical record: a replay can return only those data that could have been produced by the drilling practices and observational capabilities of the relevant era.

In the historical workflow, the concept was a short list of mutually exclusive hypotheses, each a complete narrative of the deposit. Evidence for one part of a narrative counted for or against its other parts. The lattice-based formulation encodes the same conceptual content as a set of discrete geological elements, each of which can be independently activated or deactivated in response to newly acquired observations. When framing the problem using mutually exclusive hypothesis, the drilling data yielded posterior mass concentrated with high confidence on an interpretation that correctly recovered the structural configuration but misrepresented the ore system. In the lattice representation, however, the same drilling evidence induced revision of the structural component while retaining ore-related elements. The lattice can revise the concept only among the elements on its list. An element absent from the list cannot switch on, however strongly the drilling supports it. A geologist must add it. At McLeod the list sufficed.

At McLeod, the hypotheses of 2004 placed the value of delineation at break-even. The operator stopped the program after 2005. From the same data, the lattice placed the expected value of delineation well above break-even. Continued delineation would have kept a wide margin against a fall in metal prices. The replay therefore indicates that the 2005 appraisal should have continued and the property should have been kept. The data of the time already contained the evidence of an economic deposit. Historically, that revision waited for a new team in 2006. Under the lattice the same revision follows from the drilling, without a change of team.

Declaration of competing interest

[AUTHOR: complete with the Elsevier declarations tool and paste the result here. If nothing is declared: The author declares that he has no known competing financial interests or personal relationships that could have appeared to influence the work reported in this paper.]

Funding

[AUTHOR: list the funding sources, e.g. the Stanford Mineral-X Industrial Affiliates Program, with the role of the sponsors. If none: This research did not receive any specific grant from funding agencies in the public, commercial, or not-for-profit sectors.]

Data availability

The drilling records used in this study are public: the assessment reports (GM series) and drill-hole data of the Ministère des Ressources naturelles et des Forêts du Québec, distributed through SIGEOM. The reports used are listed in Table A.1 and in the reference list. The derived data and the replay code are available from the author on request.

Declaration of generative AI and AI-assisted technologies in the manuscript preparation process

During the preparation of this work the author used Claude (Anthropic) to draft and edit text, to write and run analysis code, and to write the scripts that produced the figures. After using this tool, the author reviewed and edited the content as needed and takes full responsibility for the content of the published article.

Acknowledgements

[AUTHOR: acknowledgements, or delete this section.]

References

Adair, R.N., 2009. Technical Report on the Resource Calculation for the Bracemac-McLeod Discoveries, Matagami Project, Québec. National Instrument 43-101 Technical Report prepared for Donner Metals Ltd. (now Sphinx Resources Ltd.) by Zorayda Consulting Ltd., 24 February 2009. Filed on SEDAR, 3 April 2009, 194 pp.

Adam, E., Arnold, G., Beaudry, C., Matthews, L., Milkereit, B., Perron, G., Pineault, R., 1997. Seismic exploration for VMS deposits, Matagami, Québec. Proceedings of Exploration 97, 433–438.

Adam, E., Perron, G., Arnold, G., Matthews, L., Milkereit, B., 2003. 3D seismic imaging for VMS deposit exploration, Matagami, Quebec. In: Eaton, D.W., Milkereit, B., Salisbury, M.H. (Eds.), Hardrock Seismic Exploration. Society of Exploration Geophysicists, Geophysical Developments 10, 229–246.

Alcalde, J., Bond, C.E., Johnson, G., Butler, R.W.H., Cooper, M.A., Ellis, J.F., 2017. The importance of structural model availability on seismic interpretation. Journal of Structural Geology 97, 161–171.

Alcalde, J., Bond, C.E., Johnson, G., Kloppenburg, A., Ferrer, O., Bell, R., Ayarza, P., 2019. Fault interpretation in seismic reflection data: an experiment analysing the impact of conceptual model anchoring and vertical exaggeration. Solid Earth 10, 1651–1662.

Beaudry, C., Gaucher, E., 1986. Cartographie géologique dans la région de Matagami. Ministère de l'Énergie et des Ressources du Québec, MB 86-32.

Bodin, T., Sambridge, M., 2009. Seismic tomography with the reversible jump algorithm. Geophysical Journal International 178(3), 1411–1436.

Bond, C.E., Gibbs, A.D., Shipton, Z.K., Jones, S., 2007. What do you think this is? "Conceptual uncertainty" in geoscience interpretation. GSA Today 17(11), 4–10.

Bond, C.E., Lunn, R.J., Shipton, Z.K., Lunn, A.D., 2012. What makes an expert effective at interpreting seismic images? Geology 40(1), 75–78.

Bonham-Carter, G.F., 1994. Geographic Information Systems for Geoscientists: Modelling with GIS. Pergamon, Oxford.

Box, G.E.P., 1980. Sampling and Bayes' inference in scientific modelling and robustness. Journal of the Royal Statistical Society A 143, 383–430.

Bratvold, R.B., Bickel, J.E., Lohne, H.P., 2009. Value of information in the oil and gas industry: past, present, and future. SPE Reservoir Evaluation & Engineering 12(4), 630–638.

Bredehoeft, J.D., 2005. The conceptualization model problem — surprise. Hydrogeology Journal 13(1), 37–46.

Caers, J., Scheidt, C., Li, L. (Eds.), 2026. Decision-Making for Earth Resource Development: Quantifying Uncertainty. AGU Geophysical Monograph Series. Wiley, Hoboken.

Carr, P.M., Roy, G., 2011. Définition du gisement McLeod Deep du district minier de Matagami, canton Galinée, Québec. Xstrata Zinc, SIGEOM GM 65820.

Chopin, N., 2002. A sequential particle filter method for static models. Biometrika 89(3), 539–552.

Clark, J.R., 1983. The geology and trace element distributions of the sulfide bodies at Orchan mine, Matagami, Quebec. Ph.D. thesis, Colorado School of Mines, 450 pp.

Cotter, S.L., Roberts, G.O., Stuart, A.M., White, D., 2013. MCMC methods for functions: modifying old algorithms to make them faster. Statistical Science 28(3), 424–446.

de la Varga, M., Wellmann, J.F., 2016. Structural geologic modeling as an inference problem: a Bayesian perspective. Interpretation 4(3), SM1–SM16.

Del Moral, P., Doucet, A., Jasra, A., 2006. Sequential Monte Carlo samplers. Journal of the Royal Statistical Society Series B 68(3), 411–436.

Disini, A.F., Robertson, B.M., Claveria, R.J.R., 1998. The Mankayan Mineral District, Luzon, Philippines. In: Porter, T.M. (Ed.), Porphyry and Hydrothermal Copper and Gold Deposits: A Global Perspective. PGC Publishing, Adelaide, 75–86.

Ehrig, K., Kamenetsky, V.S., McPhie, J., Macmillan, E., Thompson, J., Kamenetsky, M., Maas, R., 2021. Staged formation of the supergiant Olympic Dam uranium deposit, Australia. Geology 49(11), 1312–1316.

Eidsvik, J., Ellefmo, S.L., 2013. The value of information in mineral exploration within a multi-Gaussian framework. Mathematical Geosciences 45(7), 777–798.

Eidsvik, J., Mukerji, T., Bhattacharjya, D., 2015. Value of Information in the Earth Sciences. Cambridge University Press.

Franklin, J.M., 1996. Volcanic-associated massive sulphide base metals. In: Eckstrand, O.R., Sinclair, W.D., Thorpe, R.I. (Eds.), Geology of Canadian Mineral Deposit Types. Geological Survey of Canada, Geology of Canada 8, 158–183.

Franklin, J.M., Lydon, J.W., Sangster, D.F., 1981. Volcanic-associated massive sulfide deposits. Economic Geology 75th Anniversary Volume, 485–627.

Froyland, G., Menabde, M., Stone, P., Hodson, D., 2018. The value of additional drilling to open pit mining projects. In: Dimitrakopoulos, R. (Ed.), Advances in Applied Strategic Mine Planning. Springer, Cham, pp. 119–138.

Galley, A.G., 2003. Composite synvolcanic intrusions associated with Precambrian VMS-related hydrothermal systems. Mineralium Deposita 38, 443–473.

Gelman, A., Shalizi, C.R., 2013. Philosophy and the practice of Bayesian statistics. British Journal of Mathematical and Statistical Psychology 66, 8–38.

Genna, D., Gaboury, D., Roy, G., 2014. The Key Tuffite, Matagami Camp, Abitibi Greenstone Belt, Canada: petrogenesis and implications for VMS formation and exploration. Mineralium Deposita 49(4), 489–512.

George, E.I., McCulloch, R.E., 1993. Variable selection via Gibbs sampling. Journal of the American Statistical Association 88(423), 881–889.

Geyer, C.J., Møller, J., 1994. Simulation procedures and likelihood inference for spatial point processes. Scandinavian Journal of Statistics 21(4), 359–373.

Gibson, H.L., Watkinson, D.H., 1990. Volcanogenic massive sulphide deposits of the Noranda cauldron and shield volcano, Quebec. In: Rive, M., et al. (Eds.), The Northwestern Quebec Polymetallic Belt. CIM Special Volume 43, 119–132.

Gibson, H.L., Morton, R.L., Hudak, G.J., 1999. Submarine volcanic processes, deposits, and environments favorable for the location of volcanic-associated massive sulfide deposits. Reviews in Economic Geology 8, 13–52.

Green, P.J., 1995. Reversible jump Markov chain Monte Carlo computation and Bayesian model determination. Biometrika 82(4), 711–732.

Hedenquist, J.W., Arribas, A., Reynolds, T.J., 1998. Evolution of an intrusion-centered hydrothermal system: Far Southeast–Lepanto porphyry and epithermal Cu-Au deposits, Philippines. Economic Geology 93, 373–404.

Holliday, J., McMillan, C., Tedder, I., 1999. Discovery of the Cadia Ridgeway gold-copper porphyry deposit. SMEDG symposium.

Hronsky, J.M.A., Groves, D.I., 2008. Science of targeting: definition, strategies, targeting and performance measurement. Australian Journal of Earth Sciences 55(1), 3–12.

Hunt, S., 2002. The discovery of structure-confined blind ore extensions to the Ladolam deposits, Lihir, PNG. In: Exploration in the Shadow of the Headframe: Getting a New Life on Lease. SMEDG–AIG–ASEG (NSW Branch) Symposium, Shore, North Sydney, 11 October 2002.

IEA (International Energy Agency), 2024. Global Critical Minerals Outlook 2024. IEA, Paris.

Institut de la statistique du Québec, 2025. Répartition du nombre de mètres forés, du coût total et du coût unitaire pour le forage carottier, selon la catégorie de dépenses, Québec, 1997-2025. Table 4538, statistique.quebec.ca.

Jafrasteh, B., Suárez, A., 2021. Objective functions from Bayesian optimization to locate additional drillholes. Computers & Geosciences 147, 104674.

Krahmann, R., 1936. The geophysical magnetometric investigations on West Witwatersrand areas between Randfontein and Potchefstroom, Transvaal. Transactions of the Geological Society of South Africa 39, 1–43.

Kreuzer, O.P., Etheridge, M.A., Guj, P., McMahon, M.E., Holden, D.J., 2008. Linking mineral deposit models to quantitative risk analysis and decision-making in exploration. Economic Geology 103(4), 829–850.

Large, R.R., 1992. Australian volcanic-hosted massive sulfide deposits: features, styles, and genetic models. Economic Geology 87, 471–510.

Lavallière, G., Guha, J., Daigneault, R., Bonenfant, A., 1994. Cheminées de sulfures massifs atypiques du gisement d'Isle-Dieu, Matagami, Québec: implications pour l'exploration. Exploration and Mining Geology 3, 109–129.

Li, P., Muir, J., Olivier, G., Yin, Z., Caers, J., 2026. Sequential efficacy of information for optimized geophysical and drilling strategies in mineral exploration. Geophysical Journal International 246(1), ggag176.

Liaghat, S., MacLean, W.H., 1992. The Key Tuffite, Matagami mining district: origin of the tuff components and mass changes. Exploration and Mining Geology 1, 197–207.

Linde, N., Renard, P., Mukerji, T., Caers, J., 2015. Geological realism in hydrogeological and geophysical inverse modeling: a review. Advances in Water Resources 86, 86–101.

Long, R.D., 2010. The Paroo Fault and the Mount Isa copper orebodies; a revised structural and evolutionary model, Mt Isa, Queensland, Australia. PhD thesis, James Cook University.

Lowell, J.D., 1968. Geology of the Kalamazoo orebody, San Manuel district, Arizona. Economic Geology 63(6), 645–654.

Lydon, J.W., 1984. Ore deposit models 8. Volcanogenic massive sulphide deposits, Part I: a descriptive model. Geoscience Canada 11(4), 195–202.

Lydon, J.W., 1988. Ore deposit models 14. Volcanogenic massive sulphide deposits, part 2: genetic models. Geoscience Canada 15, 43–65.

MacGeehan, P.J., 1978. The geochemistry of altered volcanic rocks at Matagami, Quebec: a geothermal model for massive sulphide genesis. Canadian Journal of Earth Sciences 15, 551–570.

Malinverno, A., 2002. Parsimonious Bayesian Markov chain Monte Carlo inversion in a nonlinear geophysical problem. Geophysical Journal International 151(3), 675–688.

Marjoribanks, R.W., Rutland, R.W.R., Glen, R.A., Laing, W.P., 1980. The structure and tectonic evolution of the Broken Hill region. Precambrian Research 13, 209–240.

McCuaig, T.C., Beresford, S., Hronsky, J., 2010. Translating the mineral systems approach into an effective exploration targeting system. Ore Geology Reviews 38(3), 128–138.

Mern, J., Caers, J., 2023. The Intelligent Prospector v1.0: geoscientific model development and prediction by sequential data acquisition planning with application to mineral exploration. Geoscientific Model Development 16(1), 289–313.

Mern, J., Corso, A., Burch, D., House, K., Caers, J., 2024. Intelligent Prospector v2.0: exploration drill planning under epistemic model uncertainty. arXiv preprint.

Mitchell, T.J., Beauchamp, J.J., 1988. Bayesian variable selection in linear regression. Journal of the American Statistical Association 83(404), 1023–1032.

Newton, O., Vowles, A., 2017. Geophysical overview of Lalor VMS deposit. Proceedings of Exploration 17, 619–635.

Oreskes, N., Shrader-Frechette, K., Belitz, K., 1994. Verification, validation, and confirmation of numerical models in the earth sciences. Science 263(5147), 641–646.

Park, H., Scheidt, C., Fenwick, D., Boucher, A., Caers, J., 2013. History matching and uncertainty quantification of facies models with multiple geological interpretations. Computational Geosciences 17, 609–621.

Phillips, N., 2022. Discovery of Fosterville Deeps, Victorian Gold Province: long term science. In: Formation of Gold Deposits, Modern Approaches in Solid Earth Sciences 21. Springer, Singapore, pp. 251–267. https://doi.org/10.1007/978-981-16-3081-1_21

Piché, M., Guha, J., Daigneault, R., 1993. Stratigraphic and structural aspects of the volcanic rocks of the Matagami mining camp, Quebec: implications for the Norita ore deposit. Economic Geology 88, 1542–1558.

Pierre, S., Jébrak, M., Faure, S., Roy, G., 2016. Depositional setting and structural evolution of the Archean Perseverance volcanogenic massive sulfide deposit, Matagami mining district, Quebec, Canada. Economic Geology 111, 1575–1594.

Rebek, J., 2007. Century zinc deposit update. Sydney Mineral Exploration Discussion Group (SMEDG), Sydney, 18 December 2007.

Refsgaard, J.C., Christensen, S., Sonnenborg, T.O., Seifert, D., Højberg, A.L., Troldborg, L., 2012. Review of strategies for handling geological uncertainty in groundwater flow and transport modeling. Advances in Water Resources 36, 36–50.

Reynolds, L.J., 2000. Geology of the Olympic Dam Cu-U-Au-Ag-REE deposit. In: Porter, T.M. (Ed.), Hydrothermal Iron Oxide Copper-Gold and Related Deposits, vol. 1. PGC Publishing, 93–104.

Roberts, D.E., Hudson, G.R.T., 1983. The Olympic Dam copper-uranium-gold deposit, Roxby Downs, South Australia. Economic Geology 78(5), 799–822.

Roberts, R.G., 1975. The geological setting of the Mattagami Lake Mine, Quebec: a volcanogenic massive sulfide deposit. Economic Geology 70, 115–129.

Roberts, R.G., Reardon, E.J., 1978. Alteration and ore-forming processes at Mattagami Lake Mine, Quebec. Canadian Journal of Earth Sciences 15, 1–21.

Roberts, R.J., 1960. Alinement of mining districts in north-central Nevada. USGS Professional Paper 400-B, 17–19.

Rojas, R., Feyen, L., Dassargues, A., 2008. Conceptual model uncertainty in groundwater modeling: combining generalized likelihood uncertainty estimation and Bayesian model averaging. Water Resources Research 44, W12418.

Ross, P.-S., McNicoll, V.J., Debreil, J.-A., Carr, P., 2014. Precise U-Pb geochronology of the Matagami mining camp, Abitibi Greenstone Belt, Quebec: stratigraphic constraints and implications for volcanogenic massive sulfide exploration. Economic Geology 109, 89–101.

S&P Global Market Intelligence, 2024. Average lead time almost 18 years for mines started in 2020–23. S&P Global, Commodity Insights.

Salisbury, M.H., Milkereit, B., Ascough, G., Adair, R., Matthews, L., Schmitt, D.R., Mwenifumbo, J., Eaton, D.W., Wu, J., 2000. Physical properties and seismic imaging of massive sulfides. Geophysics 65, 1882–1889.

Sambridge, M., Gallagher, K., Jackson, A., Rickwood, P., 2006. Trans-dimensional inverse problems, model comparison and the evidence. Geophysical Journal International 167(2), 528–542.

Scheidt, C., Li, L., Caers, J., 2018. Quantifying Uncertainty in Subsurface Systems. AGU Geophysical Monograph 236. Wiley, Hoboken.

Schodde, R., 2023. Exploration: Australia vs the World. MinEx Consulting, presentation at the International Mining and Resources Conference (IMARC), Sydney, 31 October 2023.

Sharpe, J.I., 1968. Geology and sulfide deposits of the Matagami area, Abitibi-East County. Quebec Department of Natural Resources, Geological Report 137.

Slack, J.F., 1993. Descriptive and grade-tonnage models for Besshi-type massive sulphide deposits. In: Kirkham, R.V., Sinclair, W.D., Thorpe, R.I., Duke, J.M. (Eds.), Mineral Deposit Modeling. Geological Association of Canada Special Paper 40, 343–371.

Soltani-Mohammadi, S., Safa, M., Sohrabian, B., 2021. Reducing uncertainty in mineralization boundary by optimally locating additional drill holes through particle swarm optimization. Natural Resources Research 30, 2067–2083.

Tarantola, A., 2006. Popper, Bayes and the inverse problem. Nature Physics 2(8), 492–494.

Telford, W.M., Geldart, L.P., Sheriff, R.E., 1990. Applied Geophysics, 2nd ed. Cambridge University Press.

Thurlow, J.G., 1981. Geology, ore deposits and applied rock geochemistry of the Buchans Group. PhD thesis, Memorial University of Newfoundland.

Voisey, C.R., Tomkins, A.G., Xing, Y., 2020. Analysis of a telescoped orogenic gold system: insights from the Fosterville deposit. Economic Geology 115(8), 1645–1664.

Webb, M., Rowston, P., 1995. The geophysics of the Ernest Henry Cu-Au deposit (N.W.) Qld. Exploration Geophysics 26(2–3), 51–59.

Wei, X., Yin, Z., Bonner, W., Caers, J., 2026. Falsification of geological hypotheses using drillholes and geophysics. Surveys in Geophysics 47(2), 289–315.

Wellmann, F., Caumon, G., 2018. 3-D structural geological models: concepts, methods, and uncertainties. Advances in Geophysics 59, 1–121.

Assessment reports (SIGEOM): GM 09221, GM 13311, GM 20511, GM 22303, GM 28608, GM 47941, GM 49061, GM 61688, GM 64243 (Dessureault, M., Roy, G., Nieminen, R., Boucher, R., 2009. Assessment report 2006-2008 delineation drilling program on the Bracemac-McLeod deposit, Matagami, Québec. Xstrata Zinc Canada).

Appendix A. The ledger of 2004

The ledger lists every item that a geologist on the McLeod property could have known at a date without drilling it, with the year from which the item was known and the document that records it (Table A.1). A deposit model dated to a year is built from the entries at or before that year. The reference model is not a source at any date. The entries are grouped by kind: A, the geology of the district and of the property; B, the deposits of the district; C, the drilling history of McLeod; D, the methods of survey and the physical properties of the rocks. The economic figures used by the value-of-information reward are given with Appendix D.

Table A.1. The ledger of 2004: each entry with the year from which it was known and its source. GM numbers are assessment reports in SIGEOM; the 2009 report is the technical report on the McLeod property;

Entry	Year	Statement	Source
A1	1965	Watson Lake Group (dacite, Watson rhyolite) / Key Tuffite / Wabassee Group (andesite then basalt, local tuffites, rare rhyolites); greenschist; thick till, outcrop absent	2009 report 6.1–6.2; MacGeehan 1978; Clark 1983
A2	1965	The Key Tuffite: laminated chert-tuff marker up to 10 m, district-wide, 1–2% Zn throughout; the deposits sit at or near it	2009 report 6.2; Liaghat and MacLean 1992
A3	1978	Synvolcanic gabbro sills inflate the pile and post-date the sulfides; the Bell River Complex is the heat source	2009 report 6.1–6.2; MacGeehan 1978; Mortensen 1993
A4	1960	Horizon strikes NW-SE; district dip about 45 SW on the south flank, 60–68 SW on the McLeod property; sub-vertical on the north flank; local variations common	GM 61688 IV-V
A5	1988	The Bracemac rhyolite, 25–60 m, with the thin Bracemac tuffite, lies in the hanging wall between the Key Tuffite and the Wabassee basalts	2009 report 5.2 (1972 entry), 6.2; GM 61688 V
A6	1963	Deposits are pyrite-sphalerite-chalcopyrite mounds and platters on the sea floor with pinnacles; roots in chlorite-talc pipes known from Perseverance (2000)	2009 report 7.0
A6b	2000	Roots within pipe facies below the sea floor as a deposit style (Perseverance)	2009 report 7.0
A7	1985	Alteration: pipe facies (chlorite-talc), proximal pipe, broad sericite; alteration cutting the Bracemac rhyolite marks hydrothermal activity	2009 report 6.2; Beaudry and Piche
A8	1965	Regional structure: the Daniel fault NW-SE, 0.5–1 km throw, off the property; a local fault unknown before 2008	2009 report 6.2
B1	2004	Ten deposits mined by 2004: 44.3 Mt at 8.8% Zn, 0.87% Cu, 27.8 g/t Ag, 0.46 g/t Au	GM 61688 IV
B3	1990	Bell Allard found and mined at 950–1,025 m: ore continues along the horizon far below the historic holes	2009 report Table 1; Nuvau history
B4	1965	Twelve deposits along the felsic bands of the district; productive strike length not yet in hand.	Nuvau district page; 2009 report Figure 29
C1	1960	The McLeod occurrence: M-6 6.95 m at 4.21% Cu, 1.17% Zn at 180–226 m; M-7 to 14 with single-component BHEM did not outline a zone; stringers with small massive sections at all levels in chlorite-talc alteration	2009 report 5.2; GM 61688 V; GM-09221, 11173
C2	1968	M-15 to 29 and BR-1 to 8 on the extensions, structures and alteration: limited success	2009 report 5.2; GM-13311, 20511, 22303
C3	1972	ASR-4 to 6: two stopped in the Bracemac rhyolite believing it the footwall	2009 report 5.2; GM-28608
C4	1988	MD-88-30 to 33 vertical to 700–900 m between McLeod and Bracemac: three barren Key Tuffite, one 22 cm of magnetite	2009 report 5.2; GM-47941, 49061
C5	2002	Noranda owns the McLeod property; the operator of 2004 is its district team	2009 report 5.2
C6	2004	MC-04-01 to 13 with stated targets, pulse EM in every hole, lithogeochemistry every 30 m; MC-04-07 14.05 m at 11.15% Zn, 2.04%	GM 61688 VI

Entry	Year	Statement	Source
		Cu; the conduit in 08 aligned with 07; dike truncations in 03; stringers in the Bracemac rhyolite in 11–13	
D1	1957	Surface EM, magnetics, gravity find conductors near surface only	2009 report 5.2, 9.0
D2a	1960	Single-component borehole EM	2009 report 5.2
D2b	2004	Pulse EM in every hole; the off-hole anomaly of MC-04-04 led to MC-04-07	GM 61688 VI
D3	1991	Lithogeochemistry discriminates the units; the chlorite index maps alteration	2009 report 6.2; GM 61688 VI
D4	before 1960	Handbook densities: rhyolite 2.6–2.7, basalt 2.8–3.0, gabbro 2.9–3.1, pyritic massive sulfide 3.5–4.5, till about 2.0	physics handbooks

Table A.2 lists the eleven deposits of the district known by 2004, from which the tonnage and grade priors of Table B.1 are fitted. The ten deposits mined by 2004 sum to 44.4 Mt, against the 44.3 Mt of entry B1.

Table A.2. The deposits of the Matagami district known by 2004, with the year from which each was known (discovery or first production). Source: the 2009 report, Table 1, page 15.

Deposit	Tonnage (Mt)	Zn (%)	Cu (%)	Ag (g/t)	Au (g/t)	Known from	Note
Matagami Lake	25.64	8.20	0.56	20.91	0.41	1957	mined 1963–88
Orchan	4.51	9.84	1.02	37.03	0.51	1963	mined 1963–82
Isle Dieu	3.05	17.85	1.01	76.63	0.46	1989	mined 1989–97, 320–610 m
Bell Allard South	0.23	9.24	1.14	37.03	0.51	1968	mined 1968–70
Bell Allard	3.59	13.67	1.25	40.55	0.69	1990	mined from 1999 at 950–1,025 m
Perseverance	5.12	15.82	1.24	29.00	0.38	2000	found 2000, 30–300 m
Norita	3.89	3.94	1.83	25.84	0.59	1976	mined 1976–97
Norita East	1.08	10.21	0.80	41.42	0.74	1992	mined 1992–96
New Hosco	1.83	1.73	1.73	10.29	0.34	1963	mined 1963–70
Garon Lake	0.47	2.17	1.46	10.29	0.34	1968	mined 1968–70
Radiore 2	0.14	1.34	1.57	8.57	0.31	1979	mined 1979–80

The gate withholds what was learned after the 2004 program. For the deposit model at the end of 2004 it withholds the drill holes of 2005 to 2012 and their logs, the pulp densities of 2007 and 2008, the fault and the barren window below it, the stacked lenses, McLeod Deep, and the reliability of borehole electromagnetics that the 2009 report states in hindsight. The deposit model of 2004 is conditioned on the 132 drill holes of the McLeod window known by the end of 2004, 19 of them with a Key Tuffite pick (Section 3.2). The five hypotheses of Figure 3 and their weights are the authors' interpretation of entries A1 to C6, confirmed entry by entry.

Appendix B. The world and its prior

B.1 The world and its frame

A world is one complete realization of the McLeod block, defined by the parameters of Table B.1 and drawn in Figure 6. Its frame is anchored at the occurrence, the Key Tuffite crossing of hole M-6. The coordinates u, v and w run along strike, down dip and perpendicular to the plane of the horizon. The horizon is the surface $w = H(u, v)$ of equation (1). The undulation Z is a stationary Gaussian surface with a Matérn covariance of range l and spread σ_Z, set to zero at the occurrence. Each massive-sulfide body is a half-ellipsoid on the horizon. The thickness at a point of the horizon is that of the thickest body there. The grades

there are those of the same body. A world keeps its fields on a grid of 25 m over 1.8 km along strike and 1.6 km down dip.

B.2 The prior

The prior of a world is the product of the distributions of Table B.1, each parameter drawn independently, with the switches drawn from equation (2). The parameters of an element enter a world only when its switch is on. The mound lens L_0 is present in every world. The sills logged in 2004 are a fixed part of every world and enter the forward model of a density sensor only. The drilling posterior therefore does not depend on them. The tonnage of a lens summed on the 20 m grid is 4/3 of its nominal tonnage in Table B.1. The semi-axes of a lens follow from a mean thickness of half its maximum, while a half-ellipsoid has a mean thickness of two thirds. The median of 1.83 Mt is therefore 2.4 Mt on the grid. In the prior draw, a world with the root and without background lenses receives one extra lens with probability ½. This branch is kept from the five-concept prior. It affects about 2.6% of the starting worlds. The birth–death proposal of Appendix C.5 removes the lens where the drilling does not support it. M

Table B.1. The parameters of a world and their prior distributions. N(m, s²), normal with mean m and standard deviation s; U(a, b), uniform between a and b; LN(median, s), lognormal with log standard deviation s. All distributions are independent. Positions are in the frame of Figure 6 from the occurrence. Sources: the attitude from ledger entry A4 (GM 61688, sections IV and V), narrowed by the 2004 drill holes (C.4); the tonnage and grades of a lens fitted to the eleven deposits of Table A.2 (2009 report, Table 1); the thickness range from the Perseverance and Isle Dieu sections (2009 report); the root's grades from the M-6 intercept (C.1); the deep-lens window from entries B3 and C4; the switch weights of the fault and the root from the weights of H3 and H2 (Figure 3); the densities from D4. † A declared modeling choice without a ledger source. ‡ A range set after the first lattice runs of October 2026: the smooth undulation on 6 October, the sheet and the flexure on 10 October, the halo on 12 October.

Description	Variable	Unit	Distribution
Strike of the horizon	σ	degree	N(117, 15²)
Dip of the horizon	δ	degree	N(64, 3²), truncated to 30–85
Offset of the horizon at the occurrence	w_0	m	N(0, 25²) †
Range of the undulation	l	m	U(200, 800) ‡
Spread of the undulation	σ_Z	m	U(5, 25) ‡
Undulation of the horizon	$Z(u, v)$	m	Gaussian, Matérn-3/2 covariance, zero at the occurrence ‡
Number of background lenses	n	–	Poisson, mean 1.35 (0.5 to 1.0 per km over 1.8 km of strike) †
Center of a background lens	(c_u, c_v)	m	U(−800, 800) along strike; U(−600, 400) down dip
Center of the mound lens L_0	(c_u, c_v)	m	uniform on a disc of radius 300 m about the occurrence †
Nominal tonnage of a lens	M	Mt	LN(1.83, 1.52), truncated to 0.05–40
Aspect of a lens (length over width)	α	–	U(1.5, 3)
Orientation of a lens	θ	degree	U(0, 180)
Maximum thickness of a lens	t	m	uniform on the thicknesses that keep length over thickness between 10 and 60 †, within 3–33
Zinc grade of a lens	z	%	LN(9.53, 0.35), truncated to 1–25
Copper grade of a lens	c	%	LN(0.91, 0.50), truncated to 0.05–6
Ore density	ρ_o	t/m³	3.5, fixed

Description	Variable	Unit	Distribution
Switch of element k	s_k	–	Bernoulli(w_k): 0.20 for the fault and the root; 0.10 for the second level and the deep lens; 0.10 † for the sheet, the flexure and the halo
Fault: position	v_c	m	U(−500, 700) †
Fault: throw	τ	m	either sign with probability ½, magnitude U(20, 100) †
Fault: dike width	δ_d	m	0 with probability ½, else U(10, 30) †
Root: radius	r_r	m	U(15, 40) †
Root: thickness	t_r	m	U(2, 8) †
Root: depth into the footwall	d_r	m	U(50, 150) †; density sensor only
Root: grades	–	%	1.2 Zn and 4.2 Cu, fixed
Second level: height above the horizon	h_s	m	U(80, 300) †
Second level: lens center	(c_u, c_v)	m	U(−600, 600) along strike; U(−400, 400) down dip
Second level: lens tonnage	M_s	Mt	LN(0.91, 1.52); aspect 2
Deep lens: center	(c_u, c_v)	m	U(−400, 400) along strike; U(500, 800) down dip; size, shape and grades as a lens
Sheet: half-length down dip	a	m	U(200, 600) ‡
Sheet: half-width	b	m	U(100, 300) ‡
Sheet: thickness	t	m	U(1, 8) ‡
Sheet: long axis from the dip direction	$\theta - 90$	degree	U(−15, 15) ‡
Sheet: center	(c_u, c_v)	m	U(−300, 300) along strike; U(100, 600) down dip ‡
Flexure: up-dip hinge	v_1	m	U(−300, 500) ‡
Flexure: down-dip hinge	v_2	m	U(v_1, 900) ‡
Flexure: slopes up and down dip	s_{up}, s_{dn}	–	U(−0.35, 0.35) each, up to 19 degrees ‡
Halo: footprint center	(c_u, c_v)	m	U(−400, 400) along strike; U(−100, 700) down dip ‡
Halo: semi-axes	a_h, b_h	m	U(200, 700); U(150, 400) ‡
Halo: thickness below the horizon	t_h	m	U(20, 150) ‡
Halo: density excess	$\Delta\rho$	t/m³	U(0.02, 0.15) ‡
Logged sills: thickness factor and density	–	–; t/m³	LN(1, 0.4); U(2.9, 3.1); density sensor only

Appendix C. The likelihood, the posterior and the sampler

This appendix states the likelihood of the drilling, the posterior over worlds and the sampler that conditions the worlds of Appendix B on the drill holes. Every constant is the value in the code of the paper's runs: the replay modules prior.py and belief.py with the hole likelihood of C.1, the lattice of seven elements, the smooth horizon prior, the grade term, the logged sills and the mixture proposal of C.5. In this appendix a world is m, the weight of world i in the ensemble is W_i, and the prior weight of element k is w_k.

C.1 The likelihood of the drilling

The data D are the informative holes served by the gate at the date. Each hole j is a polyline $x_j(s)$ sampled every 2 m of along-hole depth $s \in [0, L_j]$, with unit direction $d_j(s)$. A pick is a logged Key Tuffite crossing

with along-hole depth d_j, the apparent sulfide length t_j there and, where assayed, the length-weighted grades z_j (Zn %) and c_j (Cu %). Each pick has a quality class set by the source and reliability of its record. A class A pick comes from the operator's logs or reports of 2004 to 2005, which name the Key Tuffite or mark the horizon by massive sulfide. A class C pick comes from a historic hole (1959 to 1998) that the records of the time state crossed the horizon. Its depth is placed at the deepest logged tuff or at the first rhyolite below mafic rock. A class B record is negative evidence: the log states that the hole reached the level of the horizon and that the marker is absent, cut or displaced. The class sets the depth error of the pick: 13 m for class A and 32 m for class C.

The crossing of a world's horizon by hole j is the first sign change of $w\left(x_j(s)\right)-H\left(u\left(x_j(s)\right),v\left(x_j(s)\right)\right)$ along the polyline, located by linear interpolation. It gives the predicted depth $\hat{s}_j(m)$, the plane coordinates $\left(\hat{u}_j,\hat{v}_j\right)$ of the crossing and the predicted apparent sulfide length

$$\hat{t}_j(m)=\frac{T\left(\hat{u}_j,\hat{v}_j\right)}{max\left(\left|d_j\cdot n\right|,0.2\right)}. \tag{C.1}$$

A pick contributes the contaminated Gaussian

$$l_j(m)=\log\left[(1-\epsilon)\varphi\left(d_j;\hat{s}_j,\sigma_d\right)\varphi\left(t_j;\hat{t}_j,\sigma_t\right)+\frac{\epsilon}{L_j T_{max}}\right], \tag{C.2}$$

where $\varphi(x;\mu,\sigma)$ is the normal density, $\epsilon=0.01$ the probability of a blunder and $T_{max}=40$ m. The blunder component is uniform over the length of the hole and over sulfide lengths from 0 to 40 m. The depth error is $\sigma_d=13$ m for a class A pick and 32 m for a class C pick, the pick and the survey together. These errors are estimated by means of the nugget effect calculated from the horizon data. The length error is $\sigma_t=max\left(1.5,0.25\,t_j\right)$ m for class A and $max\left(3,0.3\,t_j\right)$ m for class C. A world whose horizon the hole does not cross receives the blunder term alone.

The blunder term represents a wrong pick in a legacy log: a mislabeled marker, a mistranscribed depth, or an interval assigned to the wrong unit. Without it a single outlying pick would give a likelihood near zero to every world whose horizon misses it by more than a few standard deviations. The posterior would then follow the worst pick of the record.

C.2 The posterior and the probability of an element

The posterior over worlds is

$$p(m\mid D)=\frac{p(m)L(D\mid m)}{p(D)},\quad p(D)=\int p(m)L(D\mid m)\,dm. \tag{C.3}$$

A concept s has posterior probability $p(s \mid D) = p(s)\dfrac{p(D \mid s)}{p(D)}$, where the marginal likelihood $p(D \mid s) = \int L(D \mid m)\, p(m \mid s)\, dm$ integrates over the base world and the parameters of the elements switched on. Summing over the 64 concepts with $s_k = 1$ gives equation (3). In odds it is

$$\frac{p(s_k = 1 \mid D)}{p(s_k = 0 \mid D)} = \frac{w_k}{1 - w_k} B_k, \; B_k = \frac{p(D \mid s_k = 1)}{p(D \mid s_k = 0)}. \tag{C.4}$$

The marginal likelihood $p(D \mid s_k = 1)$ integrates over the other six switches at their prior weights as well as over all parameters. The ratio B_k is the Bayes factor of element k. The element is more probable present than absent when $B_k > \dfrac{(1 - w_k)}{w_k}$. The sampler does not compute the marginal likelihoods. It draws worlds from $p(m \mid D)$. The share of worlds with the switch on estimates (3):

$$\hat{P}_k = \frac{1}{N} \sum_{i=1}^{N} s_k^{(i)}, \; \hat{B}_k = \frac{\hat{P}_k / (1 - \hat{P}_k)}{w_k / (1 - w_k)}. \tag{C.5}$$

C.3 The predictive distribution and the surprise score

The predictive distribution (4) is estimated over the ensemble as

$$\hat{p}(y \mid D) = \sum_{i=1}^{N} W_i \, p(y \mid m_i). \tag{C.6}$$

The surprise (5) compares $\lambda(y) = \log \hat{p}(y \mid D)$ for the observed y with the same quantity for $R = 200$ outcomes y_r. Each y_r is simulated by selecting a world k with probability W_k and drawing the observation under m_k with a fresh error. The surprise is computed on the 500 worlds the planner uses at the decision. The surprise and the information reward of each hole use a simpler observation model than the update. It assumes a depth error of 10 m, a thickness error of 1 m, a blunder probability of 0.001 and the true stratigraphic thickness at the crossing. The update uses (C.1) and (C.2). For the menu holes, at azimuth 030° and dip −65°, the apparent intercept length is 1.29 times the true thickness. The simpler model therefore inflates the surprise of a mineralized intercept. The null-control holes report true thickness. The threshold calibrated on the null controls therefore does not include this inflation.

C.4 The tempered sequential Monte Carlo sampler

The sampler is a tempered sequential Monte Carlo sampler with Metropolis–Hastings rejuvenation (Del Moral et al., 2006). The deposit model at the end of 2004 is built from the prior by raising the likelihood to a power ϕ that increases from 0 to 1,

$$\pi_\phi(m) \propto p(m)\, L(D_{2004} \mid m)^{\phi}, \; 0 = \phi_0 < \phi_1 < \ldots < \phi_T = 1, \tag{C.7}$$

starting from $N = 2{,}000$ draws from the prior. After each action of a campaign the same sampler tempers the new term alone. With D_b the data already conditioned on and y the new observation,

$$\pi_\phi(m) \propto p(m)\, L(D_b \mid m)\, L(y \mid m)^\phi, \tag{C.8}$$

starting from the equally weighted ensemble of the previous update. The base terms stay at full power. Every term of $L(D_b \mid m)$ is re-evaluated for every proposed world.

At step t the population is equally weighted at ϕ_{t-1}. The quantity l_i is the log likelihood of the tempered term for world i. The weights of a step to ϕ are

$$W_i(\phi) = \frac{\exp\{(\phi - \phi_{t-1}) l_i\}}{\sum_l \exp\{(\phi - \phi_{t-1}) l_l\}}, \quad ESS(\phi) = \left[\sum_i W_i(\phi)^2\right]^{-1}. \tag{C.9}$$

If the effective sample size $ESS(1) \geq \frac{N}{2}$ the step goes to $\phi_t = 1$. Otherwise ϕ_t is the largest ϕ with $ESS(\phi) \geq \frac{N}{2}$, found by 40 bisections between ϕ_{t-1} and 1. The 2004 build took ten steps: $\phi = 0.028$, 0.067, 0.109, 0.180, 0.300, 0.444, 0.610, 0.794, 0.989 and 1. The population is then resampled systematically. With one uniform draw U and $u_i = \frac{(U + i - 1)}{N}$, the ancestor of particle i is

$$A_i = min\left\{ j : \sum_{l \leq j} W_l(\phi_t) \geq u_i \right\}, i = 1, \ldots, N. \tag{C.10}$$

In the 2004 build 1,200 to 1,400 of the 2,000 resampled worlds were distinct at the intermediate steps.

C.5 Rejuvenation

Resampling copies the worlds that fit the drilling and removes the others. It does not create new worlds. After a few updates the ensemble would contain a handful of distinct worlds. Its spread would then understate the uncertainty the data leave. Rejuvenation restores the variety of the ensemble. Each world is changed by a sequence of proposed changes, applied in sweeps. A sweep proposes each kind of change once to every world.

A proposed change cannot simply be kept. If every proposal were accepted, the worlds would drift toward whatever the proposals favor. Random steps would spread them beyond what the data support. A proposal that adds an element would fill the ensemble with elements the drilling does not require. The acceptance probability decides which proposals are kept. It is constructed so that the ensemble remains a sample of the tempered posterior π_{ϕ_t} of Appendix C.4 after any number of changes: the share of worlds in any configuration stays equal to the posterior probability of that configuration. The changes alter the individual worlds. The distribution they sample stays the same.

A proposal changes a world m into a world m', drawn from a proposal density $q(m' \mid m)$. It is accepted with probability

$$\alpha(m, m') = min\left\{1, \frac{p(m')q(m \mid m')}{p(m)q(m' \mid m)} \cdot \frac{L(D_b \mid m')}{L(D_b \mid m)} \cdot \left[\frac{L(y \mid m')}{L(y \mid m)}\right]^{\phi_t}\right\}. \tag{C.11}$$

The acceptance probability is the product of three ratios, each comparing the proposed world with the current one. The prior ratio $\frac{p(m')}{p(m)}$ compares how plausible the two worlds are before any drilling. A world with an added element pays the prior weight of that element. A world with a larger throw pays the lower prior density of that throw. The likelihood ratio compares their fit to the drilling: the drilling already in the model, D_b, at full power, and the new observation y at the current power ϕ_t of the tempering. Every proposed world is therefore scored against all the drilling so far. The proposal ratio $\frac{q(m \mid m')}{q(m' \mid m)}$ corrects for proposals that make a change easier in one direction than in its reverse. Without it the ensemble would favor the worlds the proposals reach most easily.

A change that raises the posterior density, the product of prior and likelihood, is always accepted. A change that lowers it is accepted with a probability equal to the ratio. A slightly worse world is therefore often kept. A much worse world is seldom kept. The rule prevents two errors: (i) an element or a lens enters a world only when its gain in fit outweighs its prior charge; and (ii) a world the drilling cannot yet exclude keeps a chance of being accepted. The ensemble thus keeps the uncertainty the data leave.

The proposal ratio depends on how a change is drawn. Four kinds of proposal occur. The first kind is a symmetric step. The attitude and offset of the plane, the attributes of a background lens and the parameters of each element are shifted by a random step, as likely in one direction as in the other. The proposal ratio is then 1. Acceptance depends on the prior and the likelihood. Parameters walked on a logarithmic scale, such as tonnage or radius, add the Jacobian of that scale.

The second kind of proposal leaves the prior unchanged by construction. The undulation of the horizon is a large array of white-noise coefficients. Its proposal, the preconditioned Crank–Nicolson (pCN) step (Cotter et al., 2013), mixes the current array with an independent draw from the prior. The prior ratio and the proposal ratio then cancel. The acceptance depends on the likelihood ratio alone. The acceptance rate therefore does not fall as the array grows.

The third kind of proposal draws from the prior. A switch that turns an element on draws the parameters of the element from their prior. A birth adds a background lens drawn from its prior (Geyer and Møller, 1994; Green, 1995). The prior of the new parameters then cancels the proposal density. For a switch the acceptance reduces to the likelihood ratio times the prior odds of the element, $\frac{w_k}{(1-w_k)}$ to switch it on and

the inverse to switch it off. The prior weight of an element is thus its charge for entering a world (Section 5.3). For the fault, of prior weight 0.20, a switch on is accepted with probability $min\{1, \Lambda/4\}$, where Λ denotes the tempered likelihood ratio associated with the proposed configuration. The drilling must therefore fit four times better with the fault than without it. For the second level and the halo the drilling does not discriminate. Their likelihood ratio is 1. The switch then samples their prior weight. For a birth, the Poisson prior on the number of lenses plays the role of the weight of an element.

The fourth kind aims at worlds that small steps reach slowly. The relocation and the birth of a lens place about half of the new centers near the picks with sulfide. The mixture proposal draws a whole structural block, such as the attitude of the plane or the fault together with the mound lens, from a Gaussian mixture fitted to the current ensemble. It lets a world jump between solutions that small steps cannot connect.

For example, both a 95 m throw with a small lens and a 64 m throw with a 3.3 Mt lens are consistent with the 2004 crossing data. In the absence of the mixture proposal, each solution lineage traces back to only two to four ancestor worlds, and the ensemble fails to transition between these modes. For such targeted proposals, the Metropolis–Hastings proposal ratio corrects for the bias introduced by aiming; thus, the placement of a lens center near a pick by the proposal mechanism does not constitute evidential support for a lens at that location.

The mixture is fitted before the sweeps of a step and kept fixed during them. Each sweep therefore leaves the posterior of that step unchanged (Chopin, 2002). In the 2004 build the acceptance of the mixture proposal fell from 0.56 at the first step to 0.03 at the last as the posterior concentrated. With this proposal, independent runs agree on the position and the throw of the fault.

The size of a step sets how much a world changes and how often the change is kept. Small steps are almost always accepted but leave the world nearly as it was. Large steps change it more but are seldom accepted. The scale of each step is therefore set in the units of its parameter: degrees for an attitude, tens of meters for a position. It is then adapted between temperatures to the share of proposals accepted: halved when fewer than 15% are accepted, increased by half when more than 50% are. Both extremes waste sweeps. The number of sweeps follows the distance the ensemble must travel. The 2004 build starts from the prior, far from the posterior. It receives $K = 20$ sweeps at each temperature. A campaign update starts from the posterior of the previous action. One new hole changes that posterior little. The update receives $K = 8$ sweeps.

Appendix D. The rewards and the program pricing

The planner scores candidate actions with a reward. Two rewards are used. The first is the expected value of information (EVI) of equation (6): the expected value of the best terminal decision after the observation, minus its value before the observation, minus the cost of the action. It values an action in dollars through its effect on the terminal decision (Table 6).

The second criterion is non-monetary and is the objective used by the campaigns described in Section 6: the expected reduction in entropy of the deposit model, per unit cost, evaluated over ten operator-reported

quantities. These quantities comprise: (i) presence/absence of a lens; (ii) applicable concept; (iii–vi) the four footprint edges (east, west, down-dip, up-dip); (vii) presence/absence of a fault; (viii) presence/absence of a second lens level; (ix) tonnage class; and (x) zinc-grade class.

The two reward functions yield the same recommended action for of the decision steps: in both cases, the preferred option is the lowest-cost drillhole that intersects the horizon on the far side of the suspected fault. The main conclusions therefore do not depend on the choice of reward. The two rewards differ in detail. The information reward, information gain per unit cost, favors the cheapest informative hole. The value criterion stops drilling once a single action cannot change the decision to delineate or drop. The main text reports the campaigns under the information reward and scores their terminal decision with equation (6).

The terminal decision is to delineate or to drop. The expected value of delineation is the net value of the lens predicted by the deposit model, at 2004 metal prices and operating costs, minus the cost of the delineation program. That program is budgeted on the footprint the deposit model predicts: a 50 m grid over the predicted extent, with step-out holes to close each boundary. The realized value is the same decision rule scored on the reference model.

All costs are in 2004 Canadian dollars, at C$125 per meter of diamond core, the 2004 estimate of this study. The Institut de la statistique du Québec (2025) reports C$148 per meter for 2007. The planner follows the open-loop policy of Section 5.5: at each decision it chooses the action of largest expected value, updates the deposit model with the result and repeats.

Appendix E. The value-of-information computation

The expected value of information of equation (6) is a nested expectation. The outer expectation is over the observation the action would return. The inner expectation is over the deposit model given that observation. For a candidate action a,

$$EVI(a) = E_y\left[V(b \vee y)\right] - V(b) - c(a). \tag{E.1}$$

where b is the current deposit model, y the observation the action would return, V(b) the value of the best terminal decision under b, and c(a) the cost of the action. V(b) is the larger of the delineation value above and zero. Equation (E.1) is equation (6) written for the deposit model b in place of the data set D.

Both expectations are taken over the same ensemble, the 2,000 weighted worlds of Appendix C. The inner expectation does not need a new inference. On an observation y the posterior over worlds is the same ensemble re-weighted by the likelihood, equation (C.9) at full power, and V(b | y) is the terminal value evaluated on those re-weighted weights.

The outer expectation over y is taken by sampling. A pseudo-observation is drawn by selecting a world from the ensemble in proportion to its weight and simulating the observation the action would record under that world: a horizon crossing with its logging and sampling error. For each pseudo-observation the ensemble is re-weighted and V evaluated. The outer expectation is the average over the draws,

$$EVI(a) \approx \frac{1}{R} \sum_{r=1}^{R} V(b \vee y_r) - V(b) - c(a). \quad \text{(E.2)}$$

Re-weighting replaces a fresh inference per pseudo-observation with one likelihood pass over the ensemble, so the cost of (E.2) is R likelihood passes in place of R inversions. The likelihood pass is itself one vectorized operation: the horizon crossings of all 2,000 worlds are scored against a pseudo-observation together.

The level of estimator (E.2) varies widely, because a few worlds with the largest lenses dominate the terminal payoff. The planner uses only the ranking of the candidate actions. The level therefore does not matter. The pseudo-observations use common random numbers: every candidate action sees the same world selections and the same errors. The differences in the expected value of information (EVI) that rank the actions then vary much less than the EVI itself. The paired standard error of an EVI difference falls from about 10 MCAD to about 1 MCAD. An action costs 0.04 to 0.15 MCAD. The ranking therefore resolves differences in information value. The costs of the actions stay below the remaining Monte Carlo noise. At each decision point, the planner evaluates a subsample of 500 of the 2,000 worlds. Each world of the subsample answers once with a fresh error (R = 1). Each candidate action is therefore scored on 500 pseudo-observations.

The open-loop planner applies (E.2) once per decision: it values the terminal decision under the current deposit model, the planner takes the action of largest information reward (Appendix D), the reference model returns the observation, the deposit model updates by the sampler of Appendix C, and the planner chooses again until the budget is spent.

All computations ran on a single workstation, an AMD Ryzen 9 9950X with 16 cores and 121 GB of memory, in Python 3.12 with numpy and scipy; a GPU is not used. The parallel work, the sampler's rejuvenation sweeps and the planner's candidate evaluations, is spread over forked worker processes, one linear-algebra thread pinned to each, while the rest is serial.

The dominant cost at each decision is the update of the deposit model, the tempered re-anneal of the 2,000 worlds after the chosen action: the new likelihood term is tempered from zero to one in a few adaptive steps, each keeping the effective sample size at half the particles, with eight rejuvenation sweeps after each resample. Every term is re-evaluated for every particle at every step.

A replayed season of sixteen decisions takes about half an hour of the workstation when four to six seasons run side by side; the candidate scoring and the surprise monitor take a minute or two per decision. The deposit model at the end of 2004, 2,000 particles over twenty rejuvenation sweeps on the 132 holes of the window and their nineteen Key Tuffite picks, takes seven minutes.

Appendix F. The reference model

A new team found the deposit under a revised geological and geophysical model. From late 2006, Donner and Xstrata worked on the three premises of Section 3.3 (Adair, 2009, section 9). Holes were surveyed with three-component borehole EM where practical.

The Bracemac deposit was discovered in January 2007 based on an off-hole EM conductor. At McLeod, drill hole MC-07-22 intersected 5.0 m grading 19.3% Zn at the principal horizon at depths of approximately 600–850 m, beneath the 2004 mineralized zone. Subsequent delineation drilling on 50 m centers comprised 54 drill holes and 18 wedge holes, totaling ~45 km of drilling.

During delineation, the team interpreted a fault separating the Upper and Lower McLeod zones, with an intervening weakly mineralized window. Delineation also recognized a western zone, stacked sulfide lenses above the horizon, a laterally continuous Cu stringer zone below the horizon, and gabbro sills intruding the hanging-wall sequence. By February 2009, the combined Bracemac–McLeod indicated resource was estimated at 3.62 Mt averaging 11.5% Zn across four zones; the McLeod zone accounted for 1.88 Mt at 10.9% Zn. In 2009 and 2010, wedge holes from MC-08-34 and MCL-09-02 defined McLeod Deep at 1,085 to 1,385 m below surface (Carr and Roy, 2011). Commercial production, with Bracemac, began in May 2013. Of the features later used to define the resource, the 2004 holes had crossed one.

The reference model is a model of the deposit built from the full drilling record to 2012 and reconciled with the published resource. It is built on 20 m cells, in the following steps, each from a stated source.

1. The Key Tuffite surface is interpolated from every horizon crossing in the record, the logged intercepts of the marker from 1959 to 2012. 2. The massive and semi-massive sulfide lens is gridded from the delineation assays of 2007 to 2008. 3. The stringer pipe and the chlorite halo are placed from the alteration logged below and around the horizon. 4. The fault, a 50 m throw at the base of the 2004 zone, is placed under the 2008 holes that GM 64243 names. 5. The gabbro sills are placed from their logged positions in the hanging wall; the felsic dikes from the felsic intrusions logged beside the Key Tuffite in 13 holes, most drilled in 2007 and 2008; the glacial cover from the overburden logs and the surface.

The lens totals 3.01 Mt at 12.3% Zn. The 2009 indicated resource for the McLeod zone alone was 1.88 Mt at 10.9% Zn; the combined Bracemac-McLeod indicated resource of that year was 3.62 Mt at 11.5% Zn across four zones. The 2010 definition added McLeod Deep from the down-dip intercept of MC-08-34. The model is a model, so the replay tests a campaign against it and not against the real subsurface.

Figure F.1 shows the reference model in three dimensions, as four views of the raster: the record it is built from, the interpolated surfaces with the fault, the sulfide lens on the Key Tuffite surface, and a vertical section along dip through the occurrence.

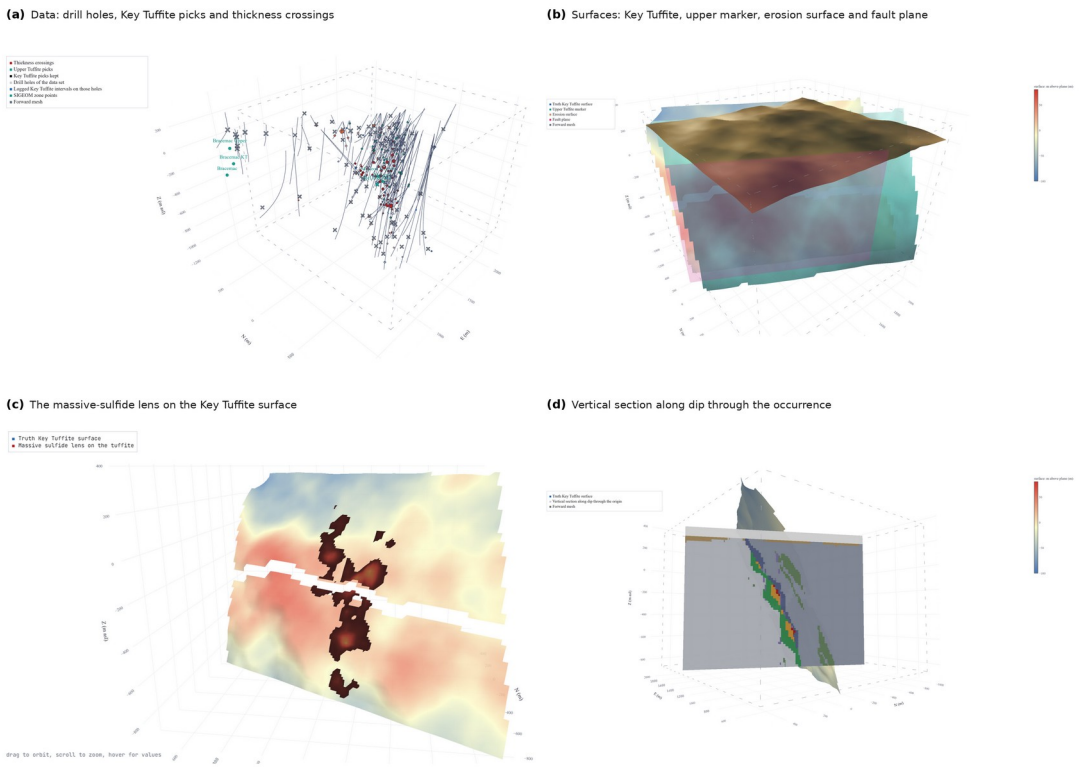


Figure F.1. The McLeod reference model in three dimensions, the four views of the model raster. (a) The record the model is built from: the drill holes of the data set, the Key Tuffite picks kept and the logged Key Tuffite intervals on those holes, the thickness crossings and the upper Tuffite picks, and the SIGEOM zone points at Bracemac. (b) The interpolated surfaces, the Truth Key Tuffite surface, the upper Tuffite marker and the erosion surface, with the fault plane and the forward mesh, the surfaces colored by height above the ledger plane. (c) The massive-sulfide lens on the Key Tuffite surface, the lens colored by its thickness. (d) A vertical section along dip through the occurrence, the units of the model on the section plane. The frame is the replay's, the origin at the M-6 occurrence.